Monthly Notices of the ROYAL ASTRONOMICAL SOCIETY

MNRAS **507,** 1296–1317 (2021) https://doi.org/10.1093/mnras/stab2189
Advance Access publication 2021 August 5

Swift/UVOT follow-up of gravitational wave alerts in the O3 era

S. R. Oates [1,2,3]★ F. E. Marshall,[4] A. A. Breeveld,[2] N. P. M. Kuin [2] P. J. Brown,[5] M. De Pasquale,[6] P. A. Evans [7] A. J. Fenney,[2] C. Gronwall,[8,9] J. A. Kennea [8] N. J. Klingler,[8] M. J. Page [2] M. H. Siegel,[8] A. Tohuvavohu,[10] E. Ambrosi,[11] S. D. Barthelmy,[4] A. P. Beardmore [7] M. G. Bernardini,[12] S. Campana,[12] R. Caputo,[4] S. B. Cenko,[4,13] G. Cusumano [11] A. D'Aì,[11] P. D'Avanzo,[12] V. D'Elia,[14,15] P. Giommi [15] D. H. Hartmann,[16] H. A. Krimm,[17] S. Laha,[4,18] D. B. Malesani,[19] A. Melandri [12] J. A. Nousek,[8] P. T. O'Brien,[7] J. P. Osborne,[7] C. Pagani,[7] K. L. Page [7] D. M. Palmer,[20] M. Perri,[14,15] J. L. Racusin,[4] T. Sakamoto,[21] B. Sbarufatti,[8,12] J. E. Schlieder,[4] G. Tagliaferri[12] and E. Troja[4,22]

Affiliations are listed at the end of the paper

Accepted 2021 July 26. Received 2021 July 26; in original form 2020 December 23

ABSTRACT

In this paper, we report on the observational performance of the *Swift* Ultra-violet/Optical Telescope (UVOT) in response to the gravitational wave (GW) alerts announced by the Advanced Laser Interferometer Gravitational Wave Observatory and the Advanced Virgo detector during the O3 period. We provide the observational strategy for follow-up of GW alerts and provide an overview of the processing and analysis of candidate optical/UV sources. For the O3 period, we also provide a statistical overview and report on serendipitous sources discovered by *Swift*/UVOT. *Swift* followed 18 GW candidate alerts, with UVOT observing a total of 424 deg^2. We found 27 sources that changed in magnitude at the 3σ level compared with archival *u*- or *g*-band catalogued values. *Swift*/UVOT also followed up a further 13 sources reported by other facilities during the O3 period. Using catalogue information, we divided these 40 sources into five initial classifications: 11 candidate active galactic nuclei (AGNs)/quasars, three cataclysmic variables (CVs), nine supernovae, 11 unidentified sources that had archival photometry, and six uncatalogued sources for which no archival photometry was available. We have no strong evidence to identify any of these transients as counterparts to the GW events. The 17 unclassified sources are likely a mix of AGN and a class of fast-evolving transient, and one source may be a CV.

Key words: gravitational waves – ultraviolet: general.

1 INTRODUCTION

The detection of the electromagnetic (EM) counterpart to gravitational wave (GW) event GW170817 (e.g. Abbott et al. 2017a, b; Coulter et al. 2017; Evans et al. 2017; Goldstein et al. 2017) marked our entry into the era of GW–EM multimessenger astronomy. With observations by a large number of dedicated telescopes and follow-up programs[1] such as were implemented at the *Neil Gehrels Swift Observatory* (henceforth *Swift*; Gehrels et al. 2004), we expect routine detection of astrophysical sources in both gravitational and electromagnetic waves. A variety of astrophysical phenomena are expected to produce GW signals, including compact binary coalescence (CBC, the coalescence of e.g. binary black hole, BBH; binary neutron stars, BNS; or black hole–neutron star, BH–NS), core-collapse supernovae (CCSN), and magnetar flares (e.g Abbott et al. 2009). The detection of GW signals together with their EM counterparts is important as it enables a more complete picture of astrophysical phenomena to be formed. Indeed, a breakthrough occurred when the first BNS GW event was detected, GW170817 (Abbott et al. 2017b, a). Associated with this GW event was a weak short gamma-ray burst (GRB) 170817A detected by the *Fermi* and Integral satellites (e.g Goldstein et al. 2017; Savchenko et al. 2017) and a bright kilonova (KN; AT2017gfo; e.g Andreoni et al. 2017; Arcavi et al. 2017; Chornock et al. 2017; Coulter et al. 2017; Cowperthwaite et al. 2017; Díaz et al. 2017; Drout et al. 2017; Evans et al. 2017; Fong et al. 2017; Gall et al. 2017; Hu et al. 2017; Kasliwal et al. 2017; Lipunov et al. 2017; McCully et al. 2017; Nicholl et al. 2017; Pian et al. 2017; Shappee et al. 2017; Smartt et al. 2017; Soares-Santos et al. 2017; Tanvir et al. 2017; Utsumi et al. 2017; Valenti et al. 2017; Villar et al. 2017; Pozanenko et al. 2018; Villar et al. 2018). Days after the GW/GRB event, an X-ray and radio counterpart emerged, which suggested that the origin was off-axis GRB afterglow emission (e.g Hallinan et al. 2017; Margutti et al. 2017; Troja et al. 2017). The association of the EM counterpart of GW170817 to the host galaxy NGC 4993 allowed the first application of GWs as standard sirens, measuring the Hubble Parameter using the distance information from the GW signal and the redshift information from the EM signal (e.g Abbott et al. 2017a, c; Guidorzi et al. 2017;

★ E-mail: sroates@star.sr.bham.ac.uk

[1]To gain an idea of the number and breadth of EM facilities following GW events, we refer the reader to Abbott et al. (2017b), which summarizes the EM follow-up of GW170817.

Palmese et al. 2017; Cantiello et al. 2018; Lee, Kang & Im 2018; Hotokezaka et al. 2019).

On 2019 April 1, the Advanced Laser Interferometer Gravitational Wave Observatory (LIGO; LIGO Scientific Collaboration; Aasi et al. 2015) and the Advanced Virgo detector (Virgo; the Virgo Scientific Collaboration; Acernese et al. 2015) began the third observing run ('O3') in search of GW events (The LIGO Scientific Collaboration and the Virgo Collaboration. 2019).[2] O3 was divided into two segments of 6 months each, separated by a month break: O3a and O3b. O3b was expected to officially end on 2020 April 30 but was cut short a month early due to the COVID-19 pandemic. One notable difference between this run and previous runs was the public release of GW alerts; in O1 and O2, the alerts were released only to the EM follow-up partners. GW triggers detected by the LIGO Scientific Collaboration and Virgo Collaboration (LVC) are assigned several parameters, including a false alarm rate (FAR; characterizing the frequency at which noise with the same strength as the signal is expected to arise), whether the detected signal arose from a CBC or an unmodelled burst, and (for CBC triggers) the estimated distance of the merger and the masses[3] of the initial compact objects. Automated preliminary notices are announced through Gamma-ray Coordinates Network (GCN) Notices[4] when analysis results in a FAR of less than 1 per 10 months or 1 per 4 yr for CBC and unmodelled burst searches, respectively. These notices are quickly followed up with a GCN Circular, released after human vetting, that provides either a confirmation of the GW alert, with an updated sky localization and source classification, or a retraction.[5]

Swift was designed specifically to detect and follow up GRBs. However, in the last few years, *Swift* has increasingly been used to explore a wide range of transient astrophysical phenomena, including the search for the EM counterpart to GW alerts. *Swift* houses three instruments: the Burst Alert Telescope (BAT; 15–350 keV; Barthelmy et al. 2005), the X-ray telescope (XRT; 0.2–10 keV; Burrows et al. 2005), and the Ultra-violet/optical Telescope (UVOT; 1600–8000 Å; Roming et al. 2005). The large field of view of the BAT, 1.4 sr (50 per cent coded), enables it to continuously view the sky and alert the spacecraft to new gamma-ray transient events such as GRBs. Once a new transient has been discovered, *Swift* rapidly slews to enable the two narrow-field instruments to observe the error region. The XRT is a focusing instrument with a peak effective area of 110 cm^2 at 1.5 keV and a roughly circular field of view with radius 11.8 arcmin. The UVOT has six optical/UV filters covering 1600–6240 Å and a *white* filter covering 1600–8000 Å, with a peak effective area of 50 cm^2 in the *u*-band. The UVOT field of view is 17×17 arcmin. Chasing the EM counterpart to a GW alert is in general difficult due to the large uncertainty in the location of these events on the sky; the probability regions released by LIGO–Virgo during O3 ranged from tens to thousands of square degrees. *Swift* has an advantage in the chase for the EM counterparts as it can respond quickly, commencing observations within a couple of hours of the GW alert, and can observe large portions of the sky within 24 h (Evans et al. 2016b; Klingler et al. 2019; Page et al. 2020). *Swift* has already shown its importance with the detection of the UV counterpart to the GW trigger 170817 by UVOT (Evans et al. 2017). BNS mergers are expected to be accompanied by a KN; red, thermal emission, produced when the ejected material, rich in neutrons, forms heavy elements through rapid neutron capture (r-process) nucleosynthesis (e.g. Lattimer & Schramm 1974; Li & Paczyński 1998; Metzger et al. 2010; Barnes & Kasen 2013; Rosswog et al. 2014; Chornock et al. 2017; Cowperthwaite et al. 2017; Drout et al. 2017; Kasliwal et al. 2017; McCully et al. 2017; Nicholl et al. 2017; Shappee et al. 2017; Smartt et al. 2017; Tanvir et al. 2017; Utsumi et al. 2017; Villar et al. 2017) and subsequently decays radioactively. High-opacity lanthanide-rich ejecta produced during the merger is expected to suppress UV and optical emission. The discovery of the UV counterpart provided the first evidence for a lanthanide-poor wind producing this blue emission (Andreoni et al. 2017; Arcavi et al. 2017; Chornock et al. 2017; Cowperthwaite et al. 2017; Díaz et al. 2017; Drout et al. 2017; Evans et al. 2017; Kasliwal et al. 2017; McCully et al. 2017; Nicholl et al. 2017; Pian et al. 2017; Smartt et al. 2017; Shappee et al. 2017; Tanvir et al. 2017; Valenti et al. 2017; Villar et al. 2017).

EM radiation is expected to be produced for both BNS and BH–NS mergers, but the emission characteristics depend on the geometry of the system. If the viewer lies close to the axis of rotation, then we expect to observe a short GRB (Eichler et al. 1989; Narayan, Paczynski & Piran 1992). The KN component is expected to be more isotropic (observed over all angles; Li & Paczyński 1998; Metzger et al. 2010). On the other hand, BBH mergers are not typically expected to produce EM radiation (Metzger 2019) but there have been predictions of EM radiation under certain circumstances, such as if accreting circumstellar material is present (see Perna, Lazzati & Farr 2019, and references therein). Graham et al. (2020) proposed the discovery of an optical EM counterpart of a BBH merger, GW190521g (Abbott et al. 2020d). For this event, the EM emission is thought to originate from the kicked BBH merger in the accretion disc of an active galactic nucleus (AGN).

There is a large diversity expected in the observed KN (Li & Paczyński 1998; Metzger 2019; Kawaguchi, Shibata & Tanaka 2020). The KN emission depends strongly on the properties of the ejecta (e.g. mass, density, and composition; Just et al. 2015), which in turn depend on the properties of the binary components (the type of merger, their masses and spins; Metzger, Thompson & Quataert 2018; Metzger 2019; Kawaguchi et al. 2020). The fate of the system post-merger also strongly affects the expected KN emission. Different KNe are expected in the BNS scenarios where the merger directly collapses to a BH, has an intermediate phase as a super/hypermassive NS, or leaves a stable NS. In the BH–NS scenario, different KNe are expected if the NS is swallowed whole or tidally disrupted (Kawaguchi et al. 2020). The observer's viewing angle may also affect the colours and luminosity of the observed KN emission (Wollaeger et al. 2018; Metzger 2019; Korobkin et al. 2021). Magnetic fields may also affect the observed emission, for instance, by enhancing winds producing the blue emission (Metzger et al. 2018) or through magnetic spin-down of a highly magnetized NS (Metzger & Piro 2014).

As AT2017gfo/GRB170817A is the only secure detection of an EM counterpart to a CBC trigger so far, each additional detection is important to further our understanding of CBCs. Studies of additional events will be crucial in gaining clear constraints on the actual range in behaviour/properties. *Swift*/UVOT is the only instrument that can provide prompt UV observations, which is critical in forming a complete picture of the EM emission associated with a GW event.

[2]On the 2020 February 25, KAGRA commenced science observations, officially joining the international network of GW detectors (Kagra Collaboration 2019).

[3]The mass estimates of the binary components were not released in the initial announcements.

[4]https://gcn.gsfc.nasa.gov/

[5]https://emfollow.docs.ligo.org/userguide/index.html

In this paper, we discuss the *Swift*/UVOT GW pipeline and the follow-up of GW alerts during O3. One effect of scanning vast areas of the sky for the EM counterpart is discovering a multitude of transient phenomena that are not necessarily related to the GW itself, and we summarize these optical transients found serendipitously during O3 in this paper. For a corresponding analysis on the X-ray observations, we refer the reader to the companion paper by Page et al. (2020), which presents the corresponding X-ray data from *Swift*. For details on the CBCs GW events observed by LIGO and Virgo during O3a (the first half of the O3 period), see the Gravitational-Wave Transient Catalog (GWTC-2; Abbott et al. 2020c). In Section 2, we briefly review the *Swift* strategy for follow-up of GW alerts and give an overview of the UVOT candidate identification pipeline. In Section 3, we provide a summary of the *Swift*/UVOT GW follow-up effort during the O3 period. Finally, in Section 4 we discuss the sources of interest found by *Swift*/UVOT during the follow-up of GW alerts in the O3 period and discuss the importance of *Swift*/UVOT in the EM follow-up of GW events. We conclude in Section 5. All uncertainties throughout this paper are quoted at 1σ unless otherwise stated. Throughout, we assume the Hubble parameter $H_0 = 70\,\mathrm{km\,s^{-1}\,Mpc^{-1}}$ and density parameters $\Omega_\Lambda = 0.7$ and $\Omega_\mathrm{m} = 0.3$. All magnitudes are given in the AB system unless otherwise stated.

2 *SWIFT* AND FOLLOW-UP OF GRAVITATIONAL WAVE SOURCES

In the ideal scenario, when GWs are emitted by merging objects, a short GRB will also be produced, which triggers the usual response by *Swift*. For this to occur, the merger should be a BNS or BH–NS, and the Earth should lie along or close to the rotation angle of the merger. However, the opening angles of the jets are expected to be narrow, between 3° and 8° (Burrows et al. 2006; Fong et al. 2015; Troja et al. 2016; Jin et al. 2018). If the jet is characterized by an angular structure, as seen in GW170817 (e.g Haggard et al. 2017; Hallinan et al. 2017; Margutti et al. 2017; Alexander et al. 2018; Lyman et al. 2018; Mooley et al. 2018; Fong et al. 2019; Ghirlanda et al. 2019; Hajela et al. 2019; Lamb et al. 2019; Troja et al. 2019, 2020), then its prompt emission could be detected for even larger viewing angles. The chance of *Swift*/BAT detecting the γ-ray emission from the short GRB resulting from the merger of a BNS or BH–NS detected by LIGO-Virgo is still very small ($\approx 0.2\,\mathrm{yr^{-1}}$; Dichiara et al. 2020). This rate becomes approximately 3 times higher with Gamma-ray Urgent Archiver for Novel Opportunities (GUANO)-targeted searches (see Tohuvavohu et al. 2020, and DeLaunay & Tohuvavohu, in preparation). FortunTately, the scheduling of *Swift* is highly flexible and responsive. Once a GW alert has been received, it can respond in a matter of hours to cover substantial portions of the GW error region with the XRT and UVOT in relatively short amounts of time in order to detect any accompanying X-ray and optical/UV emission (see Evans et al. 2016b; Klingler et al. 2019; Page et al. 2020).

2.1 *Swift* observing strategy

The longer lived EM counterpart to a GW alert (expected to be associated with a BNS or BH–NS trigger, e.g. a KN or GRB) is likely to be produced at X-ray and longer wavelengths. Therefore, the *Swift* observing strategy is optimized for follow-up with the XRT and UVOT instruments. This strategy was described in detail by Evans et al. (2016a, b), but we provide a summary here. Since the XRT and UVOT have narrow fields of view and the error region of a GW alert may cover many square degrees, many pointings (tiles) must be used to cover even a fraction of the probability region. Even with tiling, the majority of the error circle may not be covered within a reasonable time. Therefore, it is essential to try and place further constraints to prioritize regions of the sky within the GW error region. Since CBCs are expected to occur in or near galaxies, a reasonable strategy is to convolve the LVC probability region and the distance of the GW trigger with a galaxy catalogue (see section 3.2 of Evans et al. 2016b, 2019a, for further details). We use one of two catalogues: the 2MASS Photometric Redshift catalogue (2MPZ; Bilicki et al. 2014) or the Gravitational Wave Galaxy Catalogue (GWGC; White, Daw & Dhillon 2011). The GWGC catalogue is more complete compared to the 2MPZ for nearby distances (for further discussion, see Evans et al. 2016b). Therefore, we convolve the LVC probability region and the distance of the GW trigger with GWGC if the GW event is <80 Mpc and with 2MPZ if the GW event is >80 Mpc. Historically, the observing strategy was optimized to enable the greatest coverage with the XRT. This meant that some of the probability region, potentially containing host galaxies, would not fall within the UVOT field of view. However, UVOT proved to be an important discovery instrument with the UV detection of AT2017gfo (Evans et al. 2017). Therefore, a change was made to the observing strategy before the start of O3. The strategy was adjusted so that galaxies with a high probability of being the host will fall entirely within the UVOT field of view (Klingler et al. 2019).

2.1.1 *Strategy for activating* Swift *follow-up of GW events during O3*

Once a convolved probability map[6] is created, a decision can be made on whether to follow up a given GW alert. This is based on the trigger type, the FAR, and how much of the error region *Swift* can cover within 1 d. This essentially implies that *Swift* observes, primarily, events that are well localized and have a high chance of producing EM radiation, e.g. BNS merger (Evans et al. 2016b, a; Klingler et al. 2019). This strategy implicitly includes distance because the area to be tiled for nearby events will be reduced due to the galaxy convolution. Midway through the O3 period, the triggering strategy was modified to consider the probability that the trigger could have a terrestrial origin and to place stronger weight on those events where an NS is likely to have been disrupted and therefore likely to produce an EM counterpart. We summarize this updated strategy in the rest of this section. For a comparison of the strategy implemented in the O3a and O3b phases, see Page et al. (2020).

Unmodelled triggers do not require a well-known or accurate waveform model. Unmodelled triggers may be a range of transients: CBCs, CCSN, neutron star quakes, and other phenomena that may be more exotic such as cosmic strings (Abbott et al. 2009; Lynch et al. 2017). For unmodelled triggers for which the GW central frequency is >1 Hz, these events may be Galactic in origin[7] and we follow all events. If the GW signal of the unmodelled trigger is <1 Hz, these

[6]The convolved map is created from the LIGO–Virgo probability map and the galaxy catalogue.

[7]Since the power needed to create a GW signal goes as the square of the frequency, then to generate a high-frequency signal the object must either be nearby or have a lot of mass from which to generate the GW radiation strong enough to trigger LIGO–Virgo. However, with a larger mass we generally get lower frequencies (i.e. orbital periods are longer). Therefore, the most likely source of a high-frequency trigger is a very nearby stellar object, i.e. Galactic (Veitch, private communication).

are unknown, perhaps exotic objects. These events are followed only if we expect to obtain reasonable coverage, or there has been an announcement of the detection of a counterpart.

The strategy for follow-up of CBC triggers is split depending on the probability of containing a disrupted NS (DNS). The probability is determined using the following: $P_{DNS} = P_{NS}*(1 - P_{TERRES}) - P_{BHNS} + P_{REMNANT}*P_{BHNS}$ where P_{NS} is the LVC probability that the event contains an NS, P_{TERRES} is the probability that the event is terrestrial in origin (e.g. noise), and P_{BHNS} is the probability that the event is a BH–NS merger. For each trigger, P_{NS}, P_{TERRES}, P_{BHNS}, and $P_{REMNANT}$ are taken from the relevant GCN notice sent by the LVC. For BH–NS triggers, the $P_{REMNANT}$ field indicates how likely a remnant is, so we include the chance, $P_{REMNANT}*P_{BHNS}$. In this instance, $P_{DNS} = 1$ implies that an NS was disrupted and 0 implies that no NS was disrupted. The decision tree was set the following way: *Swift* would follow up an event only in the following cases:

1. For burst (unmodelled) triggers:

(a) if $\geq$1 kHz;

or (b) if $<$1 kHz and FAR $<$1/yr and well localized (50 per cent of the probability, post-galaxy convolution, is observable by XRT within 24 h).

2. For CBC triggers:

(a) if $P_{DNS} = 0$, FAR $<$1/10 yr and 50 per cent of the probability, post-galaxy convolution, is observable by XRT within 24 h;

or (b) if $0 < P_{DNS} \leq 0.25$, FAR $<$1/10 yr and 50 per cent of the probability, post-galaxy convolution, is observable by XRT within 24 h;

or (c) if $0.25 < P_{DNS} \leq 0.7$ and $>$40 per cent of the probability, post-galaxy convolution, is observable by XRT within 24 h;

or (d) if $P_{DNS} > 0.7$ and $>$10 per cent of the probability, post-galaxy convolution, is observable by XRT within 24 h.

These thresholds are set to optimize the balance between the time *Swift* dedicates to GW follow-up and the potential science return. CBC trigger types (a) and (b) typically will correspond to a BBH merger or BH–NS whereby the NS is not disrupted and may have been swallowed whole. In these cases, the expectation of observing an EM counterpart is low, but the science return is high if any emission were to be detected (e.g Metzger 2019; McKernan et al. 2019; Perna et al. 2019; Shibata & Hotokezaka 2019). In the cases where no EM emission is detected, but there is good coverage of the probability region, useful constraints can be placed on the expected emission. CBC trigger types (c) and (d) will typically correspond to a BNS or BH–NS merger whereby the NS is likely disrupted. In these cases, the expectation of observing an EM counterpart is higher. It is worth following these events even if only a low percentage of the post-galaxy convolution is observable by XRT within 24 h.

2.1.2 Swift *strategy for observing GW events*

Once a decision has been made to activate *Swift* follow-up of a GW event, the appropriate observational strategy is decided. This strategy remained the same for all trigger types until the midpoint of O3 (see Evans et al. 2016b; Klingler et al. 2019; Page et al. 2020). For the different cases of unmodelled and CBC triggers described above (Section 2.1.1), the strategy after the O3 midpoint is as follows:

1. For burst (unmodelled) triggers:

(a) Convolve LVC probability map with Galactic plane and then observe fields for 80 s each.[8] Once complete, re-observe all fields for 80 s. Keep repeating, stop only when a counterpart is found or 4 d have passed.

(b) Observe 800 fields or 90 per cent of the galaxy-convolved probability (whichever is smaller) for 80 s each. If possible, repeat observations in the same field for up to 3 d. Then, observe 500 s per field until all fields are re-observed or 4 d of these observations have been completed.

2. For CBC triggers:

(a) Follow for 24 h. If 90 per cent of the (post-galaxy convolution) probability can be observed in 48 h, then follow for 48 h.

(b) Observe 500 s per field for 4 d or until 90 per cent of the probability has been covered (whichever comes first). Do not start until 12 h after the LVC trigger time.

(c) and (d) The same strategy as for burst (unmodelled) type (b) triggers.

The CBC (b) mergers have a low probability of containing a DNS. These triggers are likely to be BBH mergers. BBH mergers are not expected to produce EM emission immediately after the trigger (if at all), and so the start of observations is delayed by 12 h. The majority of observations performed by the UVOT are with the *u* filter. This filter has the largest throughput after the *white* and *b* filters but is bluer than is typically performed by ground-based telescopes. In around 10 per cent of tiles, a less sensitive filter (e.g. *uvw*1) or the blocked filter is used to avoid damage to the instrument due to bright stars/fields.

2.1.3 Swift/*UVOT archival coverage*

The *Swift*/UVOT archive covers 15.3 per cent of the sky. In the *u* band, observations cover 8.4 per cent of the sky. Due to the vast error region of the LIGO–Virgo triggers, the likelihood of there being an archival UVOT image is small. There is a concerted effort to build an archive of local galaxies out to 100 Mpc with UVOT to have a template comparison image in the event of a nearby GW alert. The *Swift* Gravitational Wave Galaxy Survey (SGWGS; Tohuvavohu et al., in preparation) is presently observing 4773 fields, which comprise 13 000 galaxies. The survey will cover 41.8 per cent of all the catalogued *B*-band luminosity within 100 Mpc. However, the survey is optimized for the XRT, which has a larger field of view than the UVOT. Therefore, only 76 per cent of the galaxies are expected to be within the UVOT field of view. Once complete, it is expected that per GW alert with 60−100 deg^2 error region, on average, the brightest 10 galaxies in the error region will have archival images for comparison.

2.2 UVOT GW pipeline

The UVOT GW pipeline uses the standard output files produced by the processing pipeline at the *Swift* Data Centre (SDC),[9] which processes all *Swift* data. The UVOT GW processing pipeline is alerted when a new tiling observation has been processed by the SDC and is available at the SDC Quick Look website.[10] Data from that tile (a sequence) is downloaded to a Unix workstation at GSFC's Astrophysics Science Division, and the UVOT sky images are searched to identify new transient sources that might be the counterpart to the GW event. For each observation, the 'best' UVOT image is chosen (for the vast majority of tilings during the O3 period UVOT produced a single *u*-band exposure per tile) and the ftool

[8]The actual exposure time is slightly less due to the spacecraft slewing to the target, and ramp up of the photocathode in UVOT.

[9]https://swift.gsfc.nasa.gov/sdc/

[10]https://swift.gsfc.nasa.gov/sdc/ql/

Table 1. Description of the flags given to thumbnails images created for individual UVOT and XRT sources.

Quality Flag	Description
Q0	A UVOT source that passes all the quality checks and is brighter than 19.9 mag.
Q1	A UVOT source that passes all the quality checks but is fainter than 19.9 mag. There is no magnitude limit for Q1 sources as long as uvotdetect finds them.[a]
Q2	A Q0 source but with a match to a catalogued object. Matching parameters: within an angular distance of 2.5 arcsec and catalogue magnitude within 2 magnitudes of the UVOT object.
Q3	A Q1 source but with a match to a catalogued object. Matching parameters: within an angular distance of 2.5 arcsec and catalogue magnitude within 2 magnitudes of the UVOT object.
Other Flag	Description
2uvot	Q0 UVOT sources with images of current and archival UVOT exposures if available.
gal	GLADE galaxies detected in UVOT.
xrt	XRT counterparts flagged as rank 1 or rank 2 located with a UVOT image.

[a]UVOTDETECT uses a threshold of 2.0 standard deviations above the noise.

UVOTDETECT (based on SEXTRACTOR, Bertin & Arnouts 1996) is run for that exposure. All the sources found are run through a series of checks to determine if they are likely to be previously known sources, extended sources, or sources due to image artefacts. The checks include comparing the position to that of sources in the USNO-B1.0 Catalog (Monet et al. 2003) and the *HST* Guide Star Catalog II (Lasker et al. 2008), comparing the size of the major and minor axes of the source with that expected for a point source, and nearness to other bright UVOT sources. Sources due to image artefacts are avoided by comparing the position to those expected for read-out streaks and smoke rings (Breeveld et al. 2011; Page et al. 2014). Sources that pass all these initial tests are then further checked against the *Gaia* Catalog DR2 (Gaia Collaboration 2018) and the Minor Planet Checker[11]. Every source found by UVOTDETECT is assigned a Quality Flag based on the results of these checks. Sources deemed more likely to be real transients are assigned lower numbers; sources that pass all the checks are assigned a flag of 0 or 1 depending on their magnitude, referred to as Q0 or Q1 sources, respectively. Sources dimmer than a magnitude of 19.9 (a conservative sensitivity limit to obtain a signal to noise of >5 in the $\sim$80-s tiling observations) are assigned a value of 1.

The pipeline reliably finds new sources if they are isolated from existing sources and not affected by the defects in the UVOT images caused by very bright sources. However, it also produces some false detections because of the large number of UVOT sources that have to be evaluated. Consequently, the pipeline produces small images (thumbnails) for all Q0 and Q1 sources. The thumbnails allow scientists to evaluate the reliability of possible UVOT counterparts quickly. Each thumbnail has an associated flag giving the quality rating or identifying why the thumbnail was produced. The complete set of thumbnail identifiers is described in Table 1. Since the source-finding software (UVOTDETECT) sometimes misses new sources within extended sources such as nearby galaxies, thumbnails are produced for nearby galaxies reported in the GLADE catalogue (v2.3; Dálya et al. 2018)[12] that are observed with UVOT. Thumbnails are also produced for XRT counterparts categorized as rank 1 or rank 2 sources.[13]Also, if a Q0 source has an archival *Swift*/UVOT SGWGS image, a thumbnail with the quality flag '2uvot' is produced, enabling like-for-like comparison. Thumbnails were, however, not produced automatically for other archival UVOT images but were downloaded and examined during manual inspection of candidate sources. Thumbnails were also not created for sources flagged as Q2 or Q3. These are considered to be known sources.

The UVOT pipeline was modified and improved several times during O3 to reduce the number of thumbnails to check and avoid missing faint sources that may be the GW counterpart. Thumbnails for Q1 sources were added from 2019 mid-July onwards. At the same time, thumbnails for *uvw*1 images ceased to be produced as these images were found to contain a high number of false sources.

For a typical *Swift* follow-up of a GW error region covering tens of deg^2, the pipeline produces on average 2000–3000 thumbnails. The majority are thumbnails of galaxies, identified by the quality flag 'gal'. Approximately 100–200 thumbnails have other quality flags such as Q0 and Q1. During O3, UVOT performed 6441 observations and the pipeline created 18 459 thumbnails.

2.2.1 *Candidate inspection*

The thumbnails produced by the pipeline for each tile must be visually inspected to verify candidate counterparts before they are released to the community. Candidate inspection is important because scattered light artefacts (Page et al. 2014), which are inherently difficult to predict, may be misidentified as Q0 or Q1 sources. Those that are identified by eye as due to scattered light are rejected. We have newly identified a rare scattered light artefact through the manual inspection of candidates, which we label as 'ghost'. These sources are small (a few arcsec in diameter) point-like or smudge-like sources that appear on images where there is a bright source in the field of view, which produces strong scattered light features. The ghosts are likely a result of secondary reflections within the instrument. Ghosts are not expected to be produced by bright stars outside the UVOT field of view (FOV). Stars outside the FOV are instead expected to produce streaks, as observed in *XMM–Newton*–OM, but this is mitigated in UVOT by the housing. In Fig. 1, we show examples of Q0 and Q1 sources in both short ($\sim$80 s) and long ($\sim$500 s) exposures, identified as astrophysical sources and ghosts. In the examples of images containing ghosts, the ghosts are more diffuse than the neighbouring astrophysical sources and are less bright than sources of a similar dimension. Since only a handful of these artefacts have been identified, we are not yet able to automatically exclude these sources, and as such, these need to be manually rejected. A check is also made for any nearby high proper motion sources to ensure that the candidate is a new source and not an existing known source that has moved.

To look for changes in brightness in the galaxy thumbnails, difference imaging should ideally be performed. However, for the UVOT, there are only a small number of archival *u*-band UVOT images. Therefore, the thumbnails of galaxies are manually scrutinized

[11]https://cgi.minorplanetcent.net/cgi-bin/checkmp.cgi

[12]The GLADE catalogue was favoured as it was more complete than other galaxy catalogues; see fig. 4, Dálya et al. (2018).

[13]Rank 1 and rank 2 sources meet the criteria if they are uncatalogued and at least 5σ and 3σ, respectively, above the 3σ upper limit from RASS or 1SXPS, or a known X-ray source which is 5σ or 3σ above the catalogued flux.

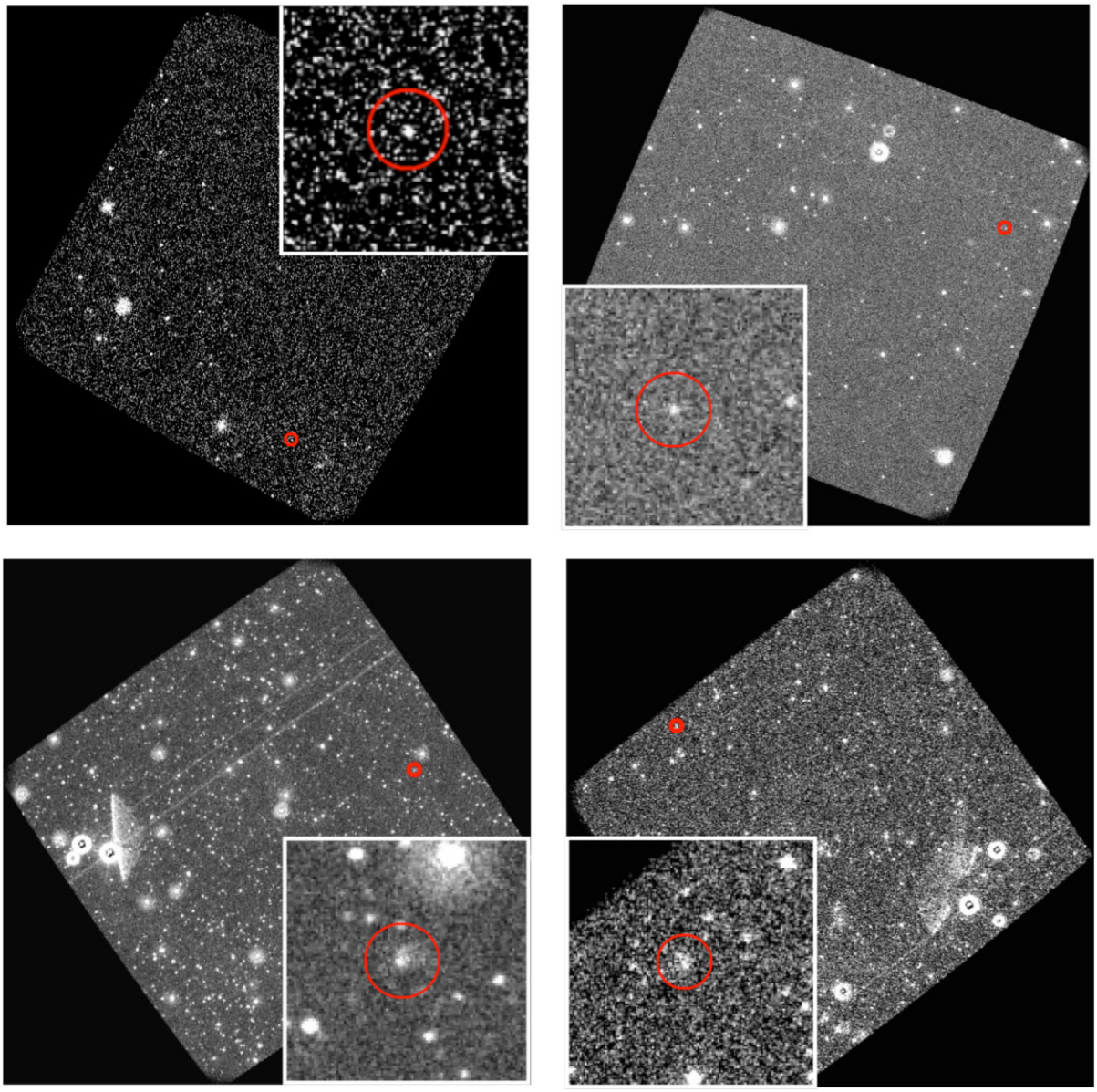

Figure 1. Examples of Q0 (left) and Q1 (right) sources. The top panels are identified as confirmed astrophysical sources, while the bottom panels are ghosts. The ghosts are scattered light features that result from secondary reflections within UVOT when there is a bright source in the field of view. The red circle indicates the location of the Q0 or Q1 source on the image. A zoom-in is provided in the insert. For the ghosts, the origin of this scattered light feature is likely the brightest source on the opposite side of the image.

for changes in brightness or any new point sources by manually comparing with the archival UVOT image if available or the DSS image.

The positions of any candidates remaining after these initial checks are cross-checked against additional archival catalogues and images (e.g. using the VizieR facility at the CDS; Ochsenbein, Bauer & Marcout 2000), including checks against the GALEX archive (Bianchi, Conti & Shiao 2014) to determine if the source is of astrophysical interest. Sources that are of immediate interest to the astronomical community, once manually vetted, are released through the GCN network. In this paper, we summarize all sources of interest that, upon manual inspection, are new sources or have a 3σ increase in brightness compared to historical values. Some of these sources were deemed to be of immediate interest to the GW–EM community and were reported via GCN circulars.

2.3 UVOT data analysis

All images were downloaded from the *Swift* data archive.[14] To determine the magnitude of a source, we use the following method. If the source is below 0.5 counts/s (c/s) and its position is known, either because it was identified by another facility or an known catalogued UV/optical/nIR source was present, we used a circular region with a 3-arcsec radius. In all other instances, we use a 5-arcsec radius. In order to be consistent with the UVOT calibration (Poole et al. 2008), count rates extracted with a 3-arcsec region were then corrected to 5 arcsec using the curve of growth contained in the *Swift* calibration files.[15] Background counts were extracted using an annular region of

[14] https://www.swift.ac.uk/archive/index.php
[15] https://heasarc.gsfc.nasa.gov/docs/heasarc/caldb/swift/

inner radius 15 arcsec and outer radius of 30 arcsec, or an aperture with a comparable area, from a blank area of sky near to the source position. The count rates were obtained from the image lists using the *Swift* tool UVOTSOURCE. Finally, the count rates were converted to AB magnitudes using the UVOT photometric zero points (Breeveld et al. 2011). The analysis pipeline used UVOT calibration 20201008. The UVOT detector is less sensitive in a few small patches[16] for which a correction has not yet been determined. Therefore, we have checked to see if any of the sources of interest fall on any of these patches in any of our images and exclude five individual UV exposures (2 for ZTF19aarykkb and 3 for ZTF19acymixu) for this reason. For sources contaminated by an underlying galaxy, we have provided background subtracted values for those that have template observations available or for which an estimate of the flux could be obtained from an offset position on the host galaxy. The details of host subtraction are provided for individual events in the supplementary section.

3 RESULTS OF *SWIFT*/UVOT FOLLOW-UP DURING THE O3 PERIOD

Of the 56 public GW alerts released by the LVC, *Swift* obtained images for 18 GW alerts. These events were selected as they met the *Swift* trigger criteria, as given in Section 2.1.1. However, two of the events were followed at the request of the *Swift* team for reasons explained below. Of these 18 events, three were retracted by the LVC, and a further three of the 18 GW alerts did not match the criteria for the Gravitational-Wave Transient Catalog (GWTC-2) of CBCs observed by LIGO and Virgo (Abbott et al. 2020c). The fraction of the LVC region tiled by UVOT varies from alert to alert. We summarize our search of all GW alerts, which had a partial or complete response in this section. A list of GW alerts followed by *Swift* along with their classification, distance, FAR, the fraction of LVC region covered by the UVOT, the number of fields observed by UVOT, and the number of thumbnails produced during automatic analysis by the UVOT software is given in Table 2. Full details of the fields observed in each case can be found under the specific trigger page at https://www.swift.ac.uk/LVC/. For the complete list of GW alerts from the third observing run, noting which were followed up by *Swift*, see Supplementary A1 of Page et al. (2020). Detailed information about the *Swift* pointings is also provided by The Gravitational Wave Treasure Map tool[17] (Wyatt et al. 2020), which is designed to visualize and coordinate EM follow-up.

3.1 GW alerts followed up with *Swift*/UVOT

In the following, we provide a summary of the individual GW triggers followed up by *Swift* during the O3 period and provide an overview of the results of the processing and inspection of UVOT images and thumbnails produced during the automatic pipeline processing. We provide the number of sources of interest determined, after manual inspection, to be astrophysical in origin and to have brightened by 3σ compared to archival values. We also provide a summary of the *Swift*/UVOT follow-up of sources discovered by other observatories. Detailed information on the individual sources, their detection, and follow-up is provided in Supplementary S.1.

For candidate sources reported by other observatories, two names may be given: the name given by the instrument team and the name given by the Transient Name Server[18], e.g. AT2019aaa. We summarize all sources of interest identified or followed up by UVOT in Table 3. We provide the UVOT photometry in Table 4 and give the XRT count rate for each source in Table 5. We note that none of the sources of interest were detected by XRT in either single exposures or a stack of all X-ray observations taken at that location.

3.1.1 S190412m/GW190412

S190412m (LIGO Scientific Collaboration & Virgo Collaboration 2019a) was identified as a BBH (>99 per cent). This event formally did not meet the *Swift* trigger criteria but was chosen to follow up as a test of the new *Swift* tiling plan ('manypoint') designed to observe many locations in a short space of time. Through further analysis, S190412m was confirmed as a highly significant GW detection and renamed GW190412, a BBH merger with asymmetric masses (The LIGO Scientific Collaboration 2020). Automatic analysis identified 13 Q0 sources. Manual inspection of the thumbnails identified three of the Q0 thumbnails as being sources of interest.

3.1.2 S190425z/GW190425

For S190425z (LIGO Scientific Collaboration & Virgo Collaboration 2019b), a high-probability BNS GW alert, automatic analysis identified 22 Q0 sources. All sources except two were ruled out through further inspection. UVOT also followed up two sources detected by the Zwicky Transient Facility (ZTF): ZTF19aarykkb and ZTF19aarzaod (Kasliwal et al. 2019) and one source from the Panoramic Survey Telescope & Rapid Response System (Pan-STARRS): AT2019ebq (PS19qp; Smith et al. 2019). Through further analysis, S190425z was confirmed as BNS with a total mass of 3.4 $M_\odot$ and renamed as GW190425 (Abbott et al. 2020a).

3.1.3 S190426c/GW190426_152155

Initial classification of S190426c (LIGO Scientific Collaboration & Virgo Collaboration 2019c) gave the probability of this event being: 49 per cent BNS merger, 24 per cent Mass Gap,[19] 14 per cent terrestrial, and 13 per cent BH–NS merger. However, this classification was updated 4 months later, indicating a 58 per cent probability of being terrestrial in origin (LIGO Scientific Collaboration & Virgo Collaboration 2019d). Automatic UVOT pipeline analysis of this candidate BNS merger identified 131 Q0 sources. The majority of these were immediately excluded as they were from a couple of images with poor aspect solution, which resulted in double or smeared stars. After manual inspection, no UVOT sources were of interest (Kuin & Swift Team 2019). *Swift* performed follow-up observations of one external candidate, ZTF19aassfws (Perley et al. 2019). In GWTC-2, this event is reported as a possible BH–NS merger and renamed GW190426_152155 (Abbott et al. 2020c).

3.1.4 S190510g

This source was initially reported as a high-probability BNS merger in LIGO Scientific Collaboration & Virgo Collaboration (2019e) but was revised more than a day later as having a high likelihood of

[16] https://heasarc.gsfc.nasa.gov/docs/heasarc/caldb/swift/docs/uvot/uvotcaldb_sss_01.pdf
[17] http://treasuremap.space/
[18] https://wis-tns.weizmann.ac.il/
[19] Mass gap implies a system with at least one compact object whose mass is in the hypothetical 'mass gap' between NS and BH, taken to be 3 and 5$M_\odot$

Table 2. The GW alerts triggering a full or partial response by *Swift* together with statistics on the UVOT response. The columns given are the LVC GW trigger name, the *Swift* identification number (ID), the GW trigger time ($T_{0,\,GW}$) in UT, the start time of the *Swift* observations in hours after trigger time, the false alarm probability per year (FAR), the sky localization (area; 90 per cent probability region), the distance to the GW and 1σ error, the number of observations performed by UVOT, the fraction of the total localization probability tiled by UVOT, the number of thumbnails produced in the UVOT GW pipeline, and the GW classification with the chance of it being a particular type of object given as a percentage in brackets. In the FAR and area columns and table notes, we identify which skymap these values were taken from BAYESTAR, LALInference, or coherent WaveBurst, respectively; see https://gracedb.ligo.org/. A large FAR value indicates a low likelihood of this event being a false event.

GW trigger	*Swift* ID	$T_{0,\,GW}$ (UT)	*Swift* obs. start time (h)	FAR (yr^{-1})[a]	Area[a] 90 per cent (deg^2)	Distance[a] (Mpc)	Number of UVOT Observations	Fraction of GW localization probability covered by UVOT	Unique area tiled by UVOT (deg^2)	Number of thumbnails	GW classification[a]
S190412m	19	05:30:44	$T_0 + 10.6$	1.88×10^{19}	156[b]	812 ± 194[b]	100	0.12	6.59	287	BBH (>99)
S190425z	22	08:18:05	$T_0 + 4.6$	6.98×10^{4}	7461	156 ± 41	406	0.01	29.22	2773	BNS (>99)
S190426c	23	15:21:55	$T_0 + 2.4$	1.63	1131	377 ± 100	894	0.13	43.77	1008	BNS (24), MassGap (12), Terrestrial (58), BH–NS (6), BBH (<1)
S190510g	25	02:59:39	$T_0 + 2.0$	3.59	1166	227 ± 92	977	0.46	55.71	2836	Terrestrial (58), BNS (42)
S190718y	39	14:35:12	$T_0 + 3.8$	1.15	7246[b]	227 ± 165[b]	368	0.12	20.88	734	Terrestrial (98), BNS (2)
S190728q	42	06:45:11	$T_0 + 12.7$	1.25×10^{15}	104	874 ± 171	144	0.22	11.23	115	BBH (95), MassGap (5)
S190808ae[R]	43	22:21:21	$T_0 + 3.4$	1.06	5365[b]	208 ± 77[b]	36	<0.01	2.91	365	Terrestrial (57), BNS (43)
S190814bv	44	21:10:39	$T_0 + 3.2$	1.55×10^{25}	23	267 ± 52	352	0.69	14.83	2488	BH–NS (>99)
S190822c[R]	46	01:29:59	$T_0 + 2.0$	5.16×10^{9}	2769[b]	35 ± 10	37	<0.01	2.91	–	BH–NS (>99), Terrestrial (<1)
S190930t	57	14:34:08	$T_0 + 2.1$	2.05	24220[b]	108 ± 38[b]	746	0.02	50.06	2479	BH–NS (74), Terrestrial (26)
S191110af[R]	61	23:06:44	$T_0 + 2.9$	12.68	1261[c]	–	797	<0.01	87.81	55	Unmodelled transient candidate
S191213g	70	04:34:08	$T_0 + 39.7$	1.12	4480	201 ± 81	4	<0.01	–	3	BNS (77), Terrestrial (23)
S191216ap	73	21:33:38	$T_0 + 6.1$	2.80×10^{15}	253	376 ± 70	113	0.02	8.01	190	BBH (99)
S200114f	82	02:08:18	$T_0 + 1.8$	25.84	403[c]	–	206	0.22	15.53	183	Unmodelled transient candidate
S200115j	83	04:23:10	$T_0 + 2.0$	1513	765	340 ± 79	512	0.03	24.08	3266	Mass Gap (>99)
S200213t	88	04:10:40	$T_0 + 5.7$	1.97	2326	201 ± 80	9	<0.01	0.62	5	BNS (63), Terrestrial (37)
S200224ca	90	22:22:34	$T_0 + 6.1$	1974	72	1575 ± 322	670	0.62	46.17	1654	BBH (>99)
S200225q	91	06:04:21	$T_0 + 47.9$	3.45	22	995 ± 188	70	0.39	2.85	18	BBH (96), Terrestrial (4)

[a]Note that these parameters are from the most recent analysis on https://gracedb.ligo.org/superevents/public/O3/ and may not necessarily be the values at the time *Swift* observations were uploaded. Area and distance parameters are from LALInference.fits.gz or are otherwise marked.
[b]Value from bayestar.fits.gz.
[c]Value from cWB.fits.gz.
[R]Retracted.

Table 3. The main properties of the sources of interest discovered or followed up with the UVOT during the search for the EM counterpart to GWs during the LIGO-Virgo O3 period. The columns are GW alert name; source ID; position in RA and Dec in degrees, J2000; peak UVOT *u*-band magnitude; change in *u*-band brightness, Δm; Galactic coordinates in degrees; and an initial classification based on a literature search. Δm is computed using the peak *u* mag and either the minimum UVOT *u*-band value, where available, or a catalogue *u*- or *g*-band value. Those using a *g*-band archival value are identified with a *g* in brackets. For the sources discovered with other facilities, we provide only Δm when it can be computed from either UVOT observations only or a UVOT *u*-band magnitude, and a catalogued *u*-band value exists. For the classifications, we use the term *uncatalogued* for sources that have not been observed previously in optical catalogues and *unidentified* when an object has archival photometry but no external classification.

GW trigger	Source ID	Position		Peak (u) magnitude	Δm	Galactic Coordinates		Classification
		RA (deg)	Dec (dec)	mag (AB)	mag	longitude (deg)	latitude (deg)	
S190412m	Q0_src10	223.91102	33.11029	20.32 ± 0.28	1.8	53.12997	62.58951	Candidate AGN
S190412m	Q0_src28	192.35297	14.90385	20.16 ± 0.28	1.4	300.62138	77.76651	Candidate AGN
S190412m	Q0_src36	214.56987	31.35459	20.01 ± 0.24	1.0	50.71475	70.62530	Candidate AGN
S190425z	Q0_src136	104.61515	− 45.72216	19.39 ± 0.32	>0.9	255.76602	− 17.90450	Uncatalogued
S190425z	Q0_src186	255.58000	− 12.48562	18.74 ± 0.18	>2.0	8.37740	17.43845	Unidentified
S190718y	Q1_src82	336.33604	− 55.99178	20.42 ± 0.16	0.7 (*g*)	334.92714	− 51.07915	Unidentified
S190814bv	Q1_src5	13.27599	− 25.38296	20.69 ± 0.16	0.9 (*g*)	135.10517	− 88.21519	Candidate AGN
S190814bv	Q1_src49	11.34316	− 24.46617	21.11 ± 0.21	1.2 (*g*)	95.44822	− 87.00837	Unidentified
S190814bv	Q1_src54	13.67442	− 24.89507	21.33 ± 0.17	0.9 (*g*)	141.26939	− 87.64981	Unidentified
S190814bv	Q1_src113	11.87052	− 24.22461	20.96 ± 0.13	0.6 (*g*)	105.65106	− 86.96269	Unidentified
S190930t	Q1_src33	154.41967	34.98805	19.14 ± 0.33	>1.6	189.78742	56.36393	Uncatalogued
S190930t	Q0_src93	334.96599	− 48.71116	19.48 ± 0.20	2.7	346.15130	− 53.71314	Unidentified
S191216ap	Q0_src147	322.0254	2.5390	17.35 ± 0.08	4.4	55.82826	− 32.77467	CV
S200114f	Q0_src201	109.68957	19.74418	17.86 ± 0.09	4.9	197.97713	14.69424	CV
S200115j	Q1_src1	43.28997	10.15932	20.30 ± 0.28	4.0 (*g*)	165.43650	− 42.44842	Unidentified
S200115j	Q1_src12	36.20419	− 6.08018	20.62 ± 0.20	1.8	173.67367	− 59.41019	Candidate AGN
S200115j	Q1_src20	36.65736	− 5.86179	20.66 ± 0.19	1.0	174.01048	− 58.94003	Candidate AGN
S200115j	Q1_src28	40.37844	− 1.37120	20.95 ± 0.30	0.9	173.26903	− 53.12805	Candidate AGN
S200115j	Q1_src39	36.19785	− 7.93239	20.84 ± 0.24	6.5	176.28980	− 60.72458	Unidentified
S200115j	Q1_src56	41.89143	5.44519	21.22 ± 0.22	1.3	168.03668	− 47.00212	Unidentified
S200115j	Q1_src58	44.39037	12.77930	21.10 ± 0.34	>0.1	164.45950	− 39.71253	Uncatalogued
S200115j	Q1_src62	36.57361	− 5.49852	21.41 ± 0.37	5.6	173.40794	− 58.73583	Unidentified
S200115j	Q1_src78	40.32801	− 2.86688	20.91 ± 0.19	1.1	174.96031	− 54.24006	Candidate AGN
S200115j	Q1_src106	36.84194	− 2.89721	20.79 ± 0.27	0.9	170.49881	− 56.63285	Candidate AGN
S200224ca	Q0_src47	176.58794	− 11.46508	19.64 ± 0.23	>2.3	278.55108	48.30150	Unidentified
S200224ca	Q1_src40	173.27717	− 2.44852	20.44 ± 0.34	0.7	267.30406	54.91160	Candidate AGN
S200224ca	Q1_src54	173.30543	− 2.46977	20.06 ± 0.32	>1.4	267.36522	54.90807	Uncatalogued
S190425z	ZTF19aarykkb	258.34145	− 9.96447	19.43 ± 0.18	–	12.13348	16.55009	SN II
S190425z	ZTF19aarzaod	262.79149	− 8.45072	21.82 ± 0.30	–	15.84702	13.59514	SN II
S190425z	PS19qp	255.32637	− 7.00289	20.25 ± 0.14	–	13.08283	20.65527	SN Ib/IIb
S190510g	Cand-A09	223.56513	4.79320	17.11 ± 0.07	>3.65	1.06508	53.19118	Uncatalogued
S190728q	ZTF19abjethn	326.39538	20.69054	16.41 ± 0.06	7.5	74.82150	− 24.35470	CV
S190814bv	AT2019osy	13.94583	− 27.07583	22.76 ± 0.33	–	210.07691	− 89.03152	Candidate AGN
S190930t	ZTF19acbpqlh	319.92166	37.52207	20.39 ± 0.09	–	83.14669	− 8.492955	SN II
S191213g	ZTF19acykzsk	32.90454	34.04135	19.76 ± 0.23	–	141.34476	− 25.94734	SN II
S191213g	ZTF19acyldun	79.19999	− 7.47871	19.40 ± 0.14	–	208.80094	− 24.42263	SN IIn
S191213g	ZTF19acymixu	90.91394	60.72825	>21.09	–	153.11430	17.92000	SN Ia
S191213g	PS19hgw	28.92475	31.41789	19.14 ± 0.20	–	138.67292	− 29.48205	SN IIb
S200213t	ZTF20aamvmzj	27.18921	51.43048	20.08 ± 0.27	>0.97	131.95909	− 10.43382	Uncatalogued
S200213t	ZTF20aanakcd	8.15705	41.31573	–[a]	–	119.13951	− 21.41749	SN IIn

[a]No observations were taken in the UVOT *u*-band.

Table 4. UVOT observations. A short summary is provided here. The full table is given in the Supplementary Table S.1.

GW trigger	Source of interest	Start time (UT)	Filter	Exposure (s)	Magnitude (AB)
S190412m	Q0_src10	2019-04-12T19:31:45	*u*	79	20.32 ± 0.28
S190412m	Q0_src10	2020-06-26T12:03:44	*u*	543	20.47 ± 0.12
S190412m	Q0_src28	2019-04-12T17:48:36	*u*	75	20.16 ± 0.28
S190412m	Q0_src28	2020-06-30T08:38:30	*u*	438	20.40 ± 0.15
S190412m	Q0_src36	2019-04-12T21:33:49	*u*	77	20.01 ± 0.24
S190412m	Q0_src36	2020-06-27T00:42:09	*u*	518	20.32 ± 0.12

being terrestrial in origin (LIGO Scientific Collaboration & Virgo Collaboration 2019f). In that time, *Swift* uploaded tiled observations of the initial error circle, and identification and inspection of sources had commenced. In those observations, there were 133 Q0 sources. The majority of these were on images with a jump in the aspect resulting in double stars or were false Q0 sources on *uvw*1 images. No sources were considered of interest after manual inspection. However, in Ohgami et al. (2021), an external candidate was reported: Cand-A09, which was observed by Subaru/Hyper Suprime-Cam. Reviewing the UVOT images, it was noted that this source was also observed during the tiling performed by UVOT; however, this source did not pass the pipeline checks in order for a thumbnail to be produced. This GW event, after reanalysis, did not meet the criteria to be included in GWTC-2 (Abbott et al. 2020c).

Table 5. The main X-ray upper limits measured with *Swift*/XRT of the sources of interest discovered or followed up with the UVOT during the search for the EM counterpart to GWs during the LIGO–Virgo O3 period. The columns are GW event; source ID; and XRT count rate upper limit in 0.3–10 keV energy range. The count to observed (absorbed) flux conversion factor is $\sim 4.3 \times 10^{-11}$ erg cm^{-2} count^{-1}, assuming a power-law index of $\Gamma = 1.7$ and an absorbing column of $N_{\rm H} = 3 \times 10^{20}$ cm^{-2}.

GW trigger	Source ID	XRT upper limits 0.3–10 keV (c/s)
S190412m	Q0_src10	5.97E-02
S190412m	Q0_src28	1.63E-01
S190412m	Q0_src36	1.10E-01
S190425z	Q0_src136	1.79E-01
S190425z	Q0_src186	8.43E-03
S190718y	Q1_src82	1.48E-02
S190814bv	Q1_src5	2.49E-02
S190814bv	Q1_src49	1.21E-02
S190814bv	Q1_src54	1.54E-02
S190814bv	Q1_src113	1.05E-02
S190930t	Q1_src33	1.13E-01
S190930t	Q0_src93	2.64E-04
S191216ap	Q0_src147	8.01E-02
S200114f	Q0_src201	1.08E-01
S200115j	Q1_src1	1.95E-02
S200115j	Q1_src12	9.47E-03
S200115j	Q1_src20	1.35E-02
S200115j	Q1_src28	5.83E-03
S200115j	Q1_src39	3.90E-03
S200115j	Q1_src56	1.13E-02
S200115j	Q1_src58	5.29E-03
S200115j	Q1_src62	4.31E-03
S200115j	Q1_src78	7.45E-03
S200115j	Q1_src106	4.52E-03
S200224ca	Q0_src47	4.75E-03
S200224ca	Q1_src40	1.04E-02
S200224ca	Q1_src54	7.90E-03
S190425z	ZTF19aarykkb	2.50E-03
S190425z	ZTF19aarzaod	3.67E-03
S190425z	PS19qp	1.16E-02
S190510g	Cand-A09	1.30E-01
S190728q	ZTF19abjethn	–
S190814bv	AT2019osy	1.96E-03
S190930t	ZTF19acbpqlh	5.28E-03
S191213g	ZTF19acykzsk	6.47E-03
S191213g	ZTF19acyldun	4.65E-03
S191213g	ZTF19acymixu	5.04E-03
S191213g	PS19hgw	1.89E-03
S200213t	ZTF20aamvmzj	6.71E-04
GW170817	AT2017gfo/GRB170817A	2.8E-04

3.1.5 S190718y

S190718y (LIGO Scientific Collaboration & Virgo Collaboration 2019g) had a high probability of being terrestrial in origin but also had a small chance of being a BNS merger. The *Swift* trigger criteria state that any GW events that are flagged as containing an NS would be followed up, so *Swift* performed tiling of this GW. Automatic analysis identified 254 Q0 sources and 28 Q1 sources. The vast majority of Q0 sources resulted from two images with jumps in spacecraft position resulting in double images. All but one of these sources were quickly discarded during manual inspection. This GW event, after reanalysis, did not meet the criteria to be included in GWTC-2 (Abbott et al. 2020c).

3.1.6 S190728q/GW190728_064510

S190728q (LIGO Scientific Collaboration & Virgo Collaboration 2019h) had a high chance of being a BBH merger and a 5 per cent chance of one of the remnants having a mass within the mass gap. Automatic analysis identified two Q0 sources and seven Q1 sources, and after manual inspection, only one Q0 source of interest remained. In GWTC-2, this event is renamed GW190728_064510 (Abbott et al. 2020c).

3.1.7 S190808ae

S190808ae (LIGO Scientific Collaboration & Virgo Collaboration 2019i) had a high chance of having a terrestrial origin (57 per cent) or being a BNS merger (43 per cent). It was retracted 4.5 h later (LIGO Scientific Collaboration & Virgo Collaboration 2019r). However, a small number of UVOT tiles were still obtained for this event. Automatic analysis identified 1 Q1 source, which was discarded upon manual inspection.

3.1.8 S190814bv/GW190814

S190814bv did not meet the *Swift* trigger criteria as it was likely a mass gap with a large error region (LIGO Scientific Collaboration & Virgo Collaboration 2019j). The probability region was reduced from 772 deg^2 to 38 deg^2, within 2 h after the trigger. Under the O3a trigger criteria for a mass-gap event to be observed, the 90 per cent of the probability in the galaxy-convolved skymap, $P_{0.9}$ must be $\leq$10 deg^2 (Page et al. 2020). Even with the reduction in the probability region, for S190814bv, $P_{0.9}$ was outside of the trigger criteria with $P_{0.9} =$ 18 deg^2. Therefore, a judgement call was made to observe this event. The classification was revised 12 h later, resulting in the most likely progenitor being a BH–NS merger (LIGO Scientific Collaboration & Virgo Collaboration 2019k), instantly meeting the trigger criteria. Automatic analysis identified 15 Q0 sources and 87 Q1 sources. Several of the Q0 sources were spurious detections caused by an image with a jump in the attitude. Upon manual inspection, only four Q1 sources were considered to be of interest. UVOT also followed up one source detected by ASKAP: ASKAP 005547-270433 (AT2019osy; Stewart et al. 2019). *Swift* observations of S190814bv will also be presented in Cenko et al. (in preparation). The LVC confirmed this event as a merger of a BH with a compact object, with it being either the lightest black hole or the heaviest NS yet discovered. This event has been renamed as GW190814 (Abbott et al. 2020e). As this GW event has the most precise localization of all events observed during O3, extensive searches for an EM counterpart have been performed from the ground too, providing stringent upper limits (e.g. Dobie et al. 2019; Gomez et al. 2019; Ackley et al. 2020; Andreoni et al. 2020).

3.1.9 S190822c

S190822c (LIGO Scientific Collaboration & Virgo Collaboration 2019i) had a high chance of having a terrestrial origin (57 per cent) or being a BNS (43 per cent). It was retracted 4.5 h later (LIGO Scientific Collaboration & Virgo Collaboration 2019r). A small number of UVOT tiles were obtained for this event. Automatic

analysis identified 1 Q1 source, which was discarded upon manual inspection.

3.1.10 S190930t

For S190930t (LIGO Scientific Collaboration & Virgo Collaboration 2019l), automatic analysis identified 130 Q0 sources and 44 Q1 sources. The vast majority of Q0 sources were due to poor settling of the spacecraft on one tile resulting in double sources. Of the remaining sources, one Q0 source, one Q1 source, and one galaxy remained as sources of interest. *Swift* also followed up one source detected by ZTF: ZTF19acbpqlh (Stein et al. 2019a). This single detector GW event, after re-analysis, did not meet the criteria to be included in GWTC-2 (Abbott et al. 2020c).

3.1.11 S191110af

S191110af was initially identified as an unmodelled transient candidate (LIGO Scientific Collaboration & Virgo Collaboration 2019m). However, further investigation of the GW data revealed it to be due to a short period with an elevated rate of instrumental artefacts in the frequency range of the trigger and was retracted (LIGO Scientific Collaboration & Virgo Collaboration 2019n). Since the retraction was not announced until 3 d later and the initial GW alert met the *Swift* GW trigger criteria, *Swift* performed tiled observations of the most probable region. As an unmodelled classification suggests a Galactic origin, *Swift* performed 797 tiled observations of the Galactic plane. The number of thumbnails produced was small compared to other GW triggers. A small number of galaxies were serendipitously observed as part of the Galactic plane tiling. The pipeline does not consider the merger classification; therefore, thumbnails were automatically produced for these galaxies and were examined for completeness. Automatic processing found 18 Q0 sources and 24 Q1 sources. Manual inspection of these sources did not reveal any sources of interest.

3.1.12 S191213g

For S191213g (LIGO Scientific Collaboration & Virgo Collaboration 2019o), due to the less than 10 per cent of the probability region being observable within 24 h, no formal tiling was initiated by *Swift*; however, a few reported sources were followed up. *Swift* observed four candidates, three reported by ZTF: ZTF19acykzsk (Andreoni et al. 2019a), ZTF19acyldun (AT2019wrt; Stein et al. 2019b), and ZTF19acymixu (AT2019wrr; Stein et al. 2019b), and one reported by Pan-STARRS: PS19hgw (AT2019wxt; McBrien et al. 2019).

3.1.13 S191216ap

This event was initially identified as a mass gap merger but was subsequently changed to a likely BBH merger (LIGO Scientific Collaboration & Virgo Collaboration 2019p, q). The *Swift* GW trigger criteria were not met for this trigger. Therefore, no tiling observations were performed. However, a neutrino was reported by IceCube (Hussain 2019; IceCube Collaboration 2019). *Swift* performed 100 observations of the overlap between the LVC and IceCube error regions. In addition, a gamma-ray sub-threshold event coincident with LIGO/Virgo and IceCube localizations was reported by HAWC (HAWC Collaboration 2019). *Swift* performed a seven-point tiling, covering 99.6 per cent of the HAWC 0.4-degree radius error circle and a further nine galaxies noted by Singer et al. (2019) as being consistent with the LIGO–Virgo and HAWC positions (Evans et al. 2019b). In these observations, there were 70 Q0 sources and four Q1 sources. However, most of the Q0 sources were due to poor settling on one image resulting in a double image of all objects in the exposure. After manual inspection, only one source was of interest.

3.1.14 S200114f

S200114f (LIGO Scientific Collaboration & Virgo Collaboration 2020a) was an unmodelled trigger. The error region was relatively small, and 206 tiles were planned. However, S200115j triggered LIGO–Virgo the following day, which took precedence and prevented the observation plan's completion. Additional analysis of the *Swift* follow-up of S200114f will also be presented by Evans et al. (in preparation). Automatic analysis of the 69 observed tiles produced thumbnails for five Q0 sources and 17 Q1 sources. After manual inspection, one Q0 source remained as a source of interest.

3.1.15 S200115j

S200115j (LIGO Scientific Collaboration & Virgo Collaboration 2020b) was classified as a mass gap merger. The localization skymap changed considerably between the initial BAYESTAR and later LALInference maps, with the error region shifting and decreasing in size; *Swift* observations were planned and initiated when only the BAYESTAR maps were available. Automatic analysis resulted in 3266 thumbnails from 512 UVOT images, with 15 Q0 sources and 110 Q1 sources. In manual inspection, 10 Q1 sources remained of interest, with additional follow-up observations performed.

3.1.16 S200213t

S200213t was identified as a BNS merger (63 per cent) with a non-negligible chance of being terrestrial in origin (37 per cent; LIGO Scientific Collaboration & Virgo Collaboration 2020c). The *Swift* GW trigger criteria were not met for this trigger. Therefore, no tiling observations were performed. However, IceCube announced the detection of one neutrino (IceCube Collaboration 2020) that was temporally and spatially coincident with the GW. *Swift* performed seven tiling observations within the error region of this neutrino event. Within these tiles, three Q0 sources were automatically identified but were rejected upon manual inspection. *Swift* also followed up two ZTF sources: ZTF20aamvmzj (AT2020cja; Kasliwal, ZTF Collaboration & GROWTH Collaboration 2020) and ZTF20aanakcd (AT2020cmr; Reusch et al. 2020).

3.1.17 S200224ca

S200224ca (LIGO Scientific Collaboration & Virgo Collaboration 2020d) was identified as a BBH merger (>99 per cent). Due to the relatively good localization, with 50 (90) per cent area within 13 (72) deg^2, this GW met the *Swift* trigger criteria. Automatic analysis found 17 Q0 and 65 Q1 sources. Of these, one Q0 source and two Q1 sources were manually identified as sources of interest. A discussion of *Swift* observations of S200224ca is also presented in Klingler et al. (2021).

3.1.18 S200225q

S200225q (LIGO Scientific Collaboration & Virgo Collaboration 2020e) was classified as a BBH merger (96 per cent). S200225q did not formally meet the *Swift* trigger criterion. However, the

LALInference skymap released 38 h later is well localized, so it was decided to do a 37-point tile to cover the 50 per cent region. This plan was interrupted by GRB200227A (Laha et al. 2020) and a second plan was initiated. A total of 70 tiles performed across the two plans. The second phase of 500-s tiles was not performed due to the delay. No Q0 or Q1 sources were identified by the UVOT pipeline.

3.2 Examination of the sources of interest

Altogether *Swift*/UVOT found or followed up 40 sources of interest, 36 of which have more than one observation, either from archives or from follow-up with UVOT or other facilities at the time of detection. The main properties of these sources are listed in Table 3 and their photometry is provided in Table 4. In the following, we investigate the properties of these sources. In this analysis, we also include AT2017gfo, the EM counterpart of GW170817, for comparison. Using catalogue information reported by VizieR, we were able to divide these 40 sources into five initial classifications: candidate AGN – source reported in the literature as confirmed or candidate AGNs/quasars (QSOs); SNe – sources that are reported as or confirmed as a supernova; CV – sources identified as cataclysmic variables; unidentified – sources that have archival photometry but are not identified; and uncatalogued – sources that have no archival photometry and have no identification. Dividing the sources into these classes, we have 11 candidate AGNs/QSOs, three CVs, nine SNe, 11 unidentified sources, and six uncatalogued sources.

3.2.1 Positions of the sources of interest

In Fig. 2, we display the positions of the 40 sources of interest on the sky in galactic coordinates. In the first panel, we colour the data points by peak u-band luminosity and in the second panel by the apparent change in magnitude (Δm). The sources are also divided by their initial classifications as given in the legend. There is no apparent correlation between source position and peak u-band magnitude or source position and Δm. Only one source of interest, a SN, is within $\pm 10^{\circ}$ of the Galactic plane.

3.2.2 Temporal behaviour of the sources of interest

In Supplementary Figs S.1–S.7, we display the light curves of the sources of interest that have more than one photometric detection from UVOT and other facilities and archives. We have not produced light curves for those sources initially classified as SNe. We display the light curves so that sources from the same class are grouped. We have collated optical photometry available in the Sloan Digital Sky Survey (SDSS; Alam et al. 2015), Canada–France–Hawaii Telescope Legacy Survey (CFHTLS; Cuillandre et al. 2012), Dark Energy Survey (DES; Abbott et al. 2018), Pan-STARRS (Chambers et al. 2016), Palomar Transient Factory (PTF; Law et al. 2009), ZTF (Bellm et al. 2019; Graham et al. 2019), and Catalina Real Time Transient Survey (CRTS; Drake et al. 2009).[20]

Light curves could be produced for 10 of the 11 candidate AGNs; a light curve for AT2019osy could not be created. This class has the light curves with the most photometric data points and includes light curves that span several years. Small changes in Δm occur on short time-scales, and larger changes occur over several years. These 10 light curves can be approximately divided into those that vary around a fixed magnitude with only small-scale variability ($\Delta m \sim 0.5$ mag) and those that tend to have this low-level, short time-scale variability but also larger, longer-term variability ($\Delta m \sim 1-2$ mag). For the CVs, we were able to produce light curves for two of the three. The data are sparse but show large changes in magnitude that occur on time-scales shorter than the AGN. For the most part, the light curves are poorly sampled for the unidentified sources compared to those of the candidate AGN, although the light curves span similar >1000-d time-scales. The typical magnitude range of the unidentified sources, ∼19−22, is similar to that observed for the candidate AGN. The light curves of both Q1_src39 (S200115j) and Q1_src62 (S200115j) are of particular interest since the minimum archival values from CFHTLS are ∼27 mag in u band, while the UVOT detection is ∼21 mag. There are also archival detections by other facilities at those locations suggesting that either these sources have slowly brightened over several years or that they intermittently brighten by several magnitudes at a time. A similar large magnitude change is also observed for Q1_src1 (S200115j), with archival g-band magnitude of 24.27 mag. For this event, a rapid two magnitude change in the i-band was caught by Pan-STARRS on a very short time-scale,

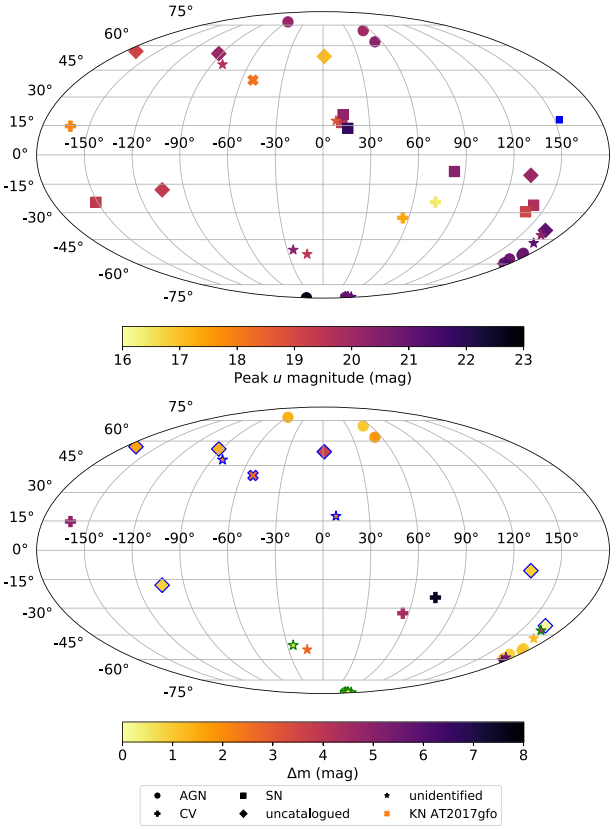

Figure 2. The positions on the sky in galactic coordinates of the 40 sources of interest detected or followed up by UVOT during O3. The colours represent the peak u-band magnitude (AB; top panel) and the change in magnitude, Δm (bottom panel), where Δm is calculated using two UVOT u exposures or the UVOT detection magnitude and an archival g-band magnitude. For the panels displaying peak u magnitudes, we have coloured objects blue where UVOT measured only an upper limit. For the panels displaying Δm, we use a blue edge to denote lower limits and a green edge to denote where change was calculated using UVOT u- and an archival g-band magnitude. Different symbols separate the sources into five categories: candidate AGN, supernovae, cataclysmic variables, unidentified, and uncatalogued, with the key given in the legend.

[20] We cross-matched using a search radius of 2 arcsec for all optical catalogues except for CRTS, which we used 3 arcsec.

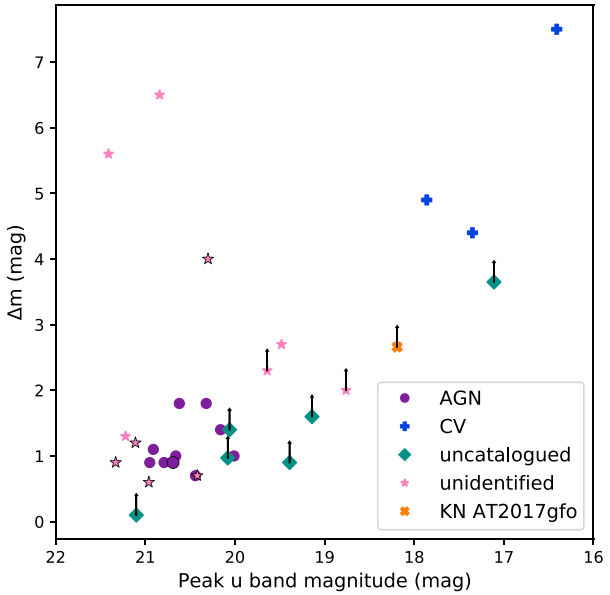

Figure 3. The peak u-band magnitude (AB) versus the change in magnitude, Δm. Δm is calculated using two UVOT u exposures or the UVOT detection magnitude and an archival g-band magnitude. The sources displayed are divided into the categories: candidate AGN, cataclysmic variables, unidentified and uncatalogued, see legend for colours and symbols. Arrows indicate lower limits to Δm, and points with a black outline indicate those points where Δm was calculated using an archival g-band magnitude rather than a UVOT u-band image. We also display the peak u-band magnitude versus Δm for AT2017gfo, the EM counterpart to GW170817.

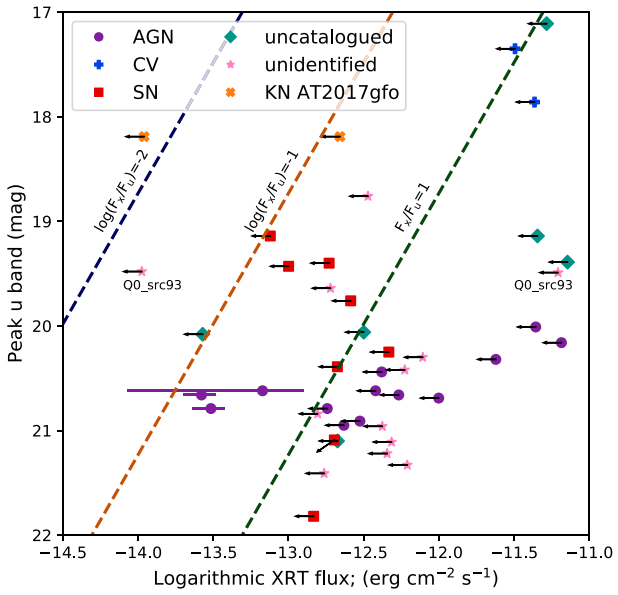

Figure 4. The X-ray flux (er g cm^{-2} s^{-1}) versus the peak u-band magnitude. The X-ray flux values measured by XRT are all in the energy range of 0.3–10 keV and are all 3σ upper limits. These values were determined from the XRT count rate using a count to observe (absorbed) flux conversion factor of $\sim 4.3 \times 10^{-11}$ erg cm^{-2} count^{-1}, calculated assuming a power-law index of $\Gamma = 1.7$ and an absorbing column of $N_{\rm H} = 3 \times 10^{20}$ cm^{-2}. For AT2017gfo associated with GW170817 and for Q0_src93, we provide two points with two different XRT upper limits: one upper limit derived from the first observation and the second deeper limit is determined from a stack of all XRT observations. In this figure, we also include archival *XMM–Newton* (0.2–12 keV; purple) flux values for three of the candidate AGN sources (Webb et al. 2020). The corresponding XRT upper limits for these three sources are shallower and are immediately to the right. The sources are separated into five initial categories: candidate AGN (circle), SNe (square), CVs (plus), unidentified (star), and uncatalogued (diamond). Sources with diagonal arrows indicate that both the X-ray flux and the peak u-band magnitude are upper limits. The diagonal dotted lines represent lines of proportionality with the optical flux 0.1 (blue), 10 (orange), and 100 (green) times the X-ray flux, with the ratio $F_{\rm u}/F_{\rm x}$ computed using the optical flux in $\nu F\nu$ and the X-ray flux in the 0.3–10 keV energy range.

around 20 min. For the uncatalogued sources, none of those first detected by UVOT have enough photometry available to produce light curves. We were, however, able to produce a light curve for one uncatalogued source, which ZTF initially identified during S200213t: ZTF20aamvmzj, see Supplementary Fig. S.7. Interestingly, the r and i data reported by Kasliwal et al. (2020) are approximately flat between the two epochs, whereas the UVOT data appear to decay. By normalizing all filters to the v band, we measure a decay slope of -1.45 ± 0.23. This is in sharp contrast to the decay slope of $\alpha = 0.04$ in the r band reported by Kasliwal et al. (2020). This difference suggests a fast decay of the source at UV wavelengths.

In Fig. 3, we display the peak u-band magnitude against Δm. Those sources identified as candidate AGN are clustered between 20th and 21st magnitude with Δm between 0.5 and 2 magnitudes. The three CVs lie in the top right corner having the brightest peak u-band magnitudes and the largest Δm. The sources classified as unidentified appear to cluster into three areas: one group is similar to that of the AGN but on average is fainter ($\geq$21 mag), the second group lies to the top right of the AGN, they are brighter between 19th and 20th mag and have $\Delta m > 1.5$ mag (Q0_src186, Q0_src93, and Q0_src47; from GW events S190425z, S190930t, and S200224ca, respectively), which lies at a similar position at AT2017gfo, and the third group lies in the top left corner, consisting of three sources with $\Delta m > 4$ and low peak u-band values (Q1_src1, Q1_src39, and Q1_src62, all from S200115j). Five of the uncatalogued sources have $\Delta m < 2$ and are between 19 and 21.5 mag. The sixth uncatalogued source appears to be as bright and has as large a change in magnitude as the CVs. No SNe are displayed since no Δm can be computed from the available data.

In Fig. 4, we display the peak u-band magnitude against the observed XRT X-ray (0.3–10 keV) flux, where the observed X-ray flux is computed using a power-law index of $\Gamma = 1.7$ and an absorbing column of $N_{\rm H} = 3 \times 10^{20}$ cm^{-2}. Three of the candidate AGNs have archival X-ray detections from *XMM–Newton* (Webb et al. 2020), which we also include. Since none of the sources are detected by XRT, all the XRT flux values are upper limits. For the most part, these upper limits are reasonably shallow. Only two sources lie below $\log(F_{\rm x}/F_{\rm u}) = -1$, one uncatalogued source (ZTF20aamvmzj; S200213t) and one unidentified source (Q0_src93; S190930t), likely excluding these two sources as resulting from an AGN. AT2017gfo, the EM counterpart of GW170817, has an even sharper contrast between the X-ray and optical flux with $\log(F_{\rm x}/F_{\rm u}) < -2$.

We have also cross-matched our sources against the ALLWISE catalogue (Cutri et al. 2021) using a search radius of 6 arcsec. In Fig. 5, we display W2–W3 versus W1–W2 colours of 16 sources of interest. Overlaid on this figure are regions indicating locations of particular types of IR objects (Wright et al. 2010); we also display 10 k AGNs determined using the completeness criteria of 75 per cent from Assef et al. (2018) that also have detections in the three WISE bands. The sources of interest are inconsistent with being stars, cool T-dwarfs, ellipticals, and obscured AGN. Almost all of the sources for which there is a WISE match are found in the luminous infrared

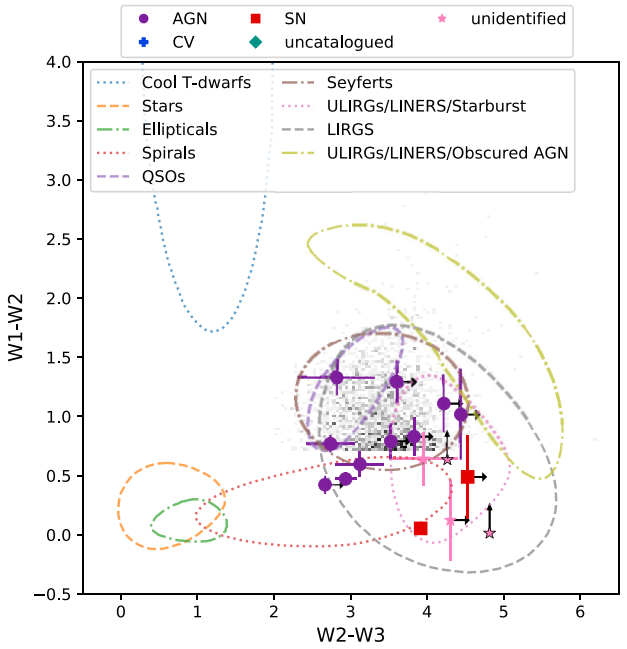

Figure 5. Colour–colour diagram of ALLWISE catalogued sources cross-matched with the UVOT sources of interest. We show the UVOT sources of interest separated into five initial categories (see legend) along with a histogram of 10^5 of the 35×10^6 ALLWISE AGN candidates from Assef et al. (2018), selected using a completeness criteria of 75 per cent (grey scale). In addition, we have overlaid the expected locations of different classes of WISE objects as given in fig. 12 of Wright et al. (2010). The two points outlined in black are detected in the WISE W1 filter only. Most of the UVOT sources of interest show consistency with the LIRG class of objects.

galaxy (LIRG) colour region. The sources in this region are a mixture of AGN (Seyferts and QSOs) and star-forming galaxies. This is strong evidence that all of the transient sources with WISE matches are extragalactic. Some of these transient sources are candidate AGNs, while others are SNe, with the WISE colours indicating that they are located in star-forming galaxies. The unidentified sources with WISE matches are likely to fall into one of these two categories.

In Fig. 6, we provide two plots displaying the colours of the objects. We have used archival photometry from SDSS, CFHTLS, DES, and stacked exposures from Pan-STARRS. The first panel, adapted from Lawrence et al. (2016), displays $u-g$ versus $g-r$ with regions identifying objects as red, blue, and ultra-blue. The grey region indicates the colour location of 90 per cent of SDSS spectroscopic quasars (see Lawrence et al. 2016, for details). In addition, we also display a 2D histogram, given in grey, of the SDSS colours of 10 000 stars from the *Gaia* DR2 catalogue, selected from a region at high Galactic latitude. Of the sources of interest, six are found in one or more catalogues, and these points are joined by red lines, indicating spectral evolution and that colour depends on the time of observation. We label some of the sources that may be of interest to the reader. Some of the candidate AGNs are consistent with the quasar region, while the others are more scattered in their position in colour. Of the candidate AGNs, two are of particular interest, both of which have two data points. Q0_src36 (S190412m) moves between being blue and ultra-blue, while Q1_src12 (S200115j) is the only AGN consistent with being red. Four other sources lie in the red section. Three of these are Q1_src39, Q1_src56, and Q1_src62 (all from S200115j); however, the errors on these are large. The fourth object is AT2017gfo, the KN associated with GW170817, which is initially blue and later becomes red. The second panel displays $g-r$ versus $r-g$. In this panel, we also display a grey region typical of the colours of quasars and the grey histogram providing the colours of stars. The blue region represents the location of the blue cloud galaxies, and the red region represents the red-sequence galaxies, both out to $z = 0.22$ (adapted from Lawrence et al. 2016). Due to more facilities observing in g, r, and i, there are more sources of interest with archival observations and many sources are found in more than one catalogue; red lines connect these. Most of the points avoid the red region, which corresponds to low-redshift elliptical galaxies. This suggests that apart from the AGN (for which we can say little about the host galaxies), the extragalactic transients identified by our survey are primarily located in star-forming galaxies. This observation may prove useful in our follow-up to future GW observing runs. The UVOT u-band survey is almost devoid of serendipitous transients in nearby elliptical galaxies, but we expect that some BNS mergers take place in these environments, because short GRBs have been observed to come from elliptical galaxies as well as star-forming galaxies (e.g. Gehrels et al. 2005; Fong et al. 2013). Therefore, UVOT transients found in elliptical galaxies should be prioritized in future GW observing runs.

4 DISCUSSION

Overall, 18 LIGO/Virgo GW triggers were followed up at differing extents by *Swift*/UVOT. Of these 18 candidate GW events, four were initially classified as BBH triggers, six as BNS events, two each of BH–NS and mass-gap triggers, one unmodelled/burst trigger, and the remaining three were subsequently retracted. Of the 10 events occurring in O3a, only five meet the criteria to be included in the GWTC-2 catalogue of O3a (Abbott et al. 2020c). Within the 6.4k UVOT tiles obtained by *Swift* across the 18 GW events, automatic analysis found a total of 828 Q0 sources and 344 Q1 sources, and after manual inspection, nine Q0 and 18 Q1 sources were considered to be of interest. None of these were considered to be EM counterparts of the GW events when they were detected. In the following, we will discuss the importance of UVOT in the search for the EM counterpart to GWs, explore the serendipitously discovered sources of interest, and discuss future improvements that can be made to UVOT's performance in detecting and following EM counterparts to GWs.

4.1 Expected optical/UV emission from KNe and UVOT

Detecting optical/UV (blue) emission from future KNe can be a particularly useful tool in determining the properties of the merged binary system. It is expected that ejecta with electron fraction $Y_e > 0.25$ will produce the blue part of the KN. The merger remnant and its duration of survival are linked to the total binary mass of the merger (Metzger 2019). The longer the merger remnant survives, the larger the expected ejecta mass with electron fraction $Y_e > 0.25$ and thus the brighter the KN in the optical/UV (Metzger & Fernández 2014; Perego et al. 2014; Lippuner et al. 2017; Metzger 2017). For BNS mergers with the largest total binary mass, the remnant will undergo prompt collapse to a BH. The fraction of material with $Y_e > 0.25$ is expected to be small, and the resulting KN is expected to be red and dimmer than AT2017gfo. For increasingly smaller total BNS masses, the merger remnants are expected to be hypermassive (HMNS), supermassive (SMNS) remnants (Metzger 2019; Shibata & Hotokezaka 2019), for which the stability before collapse is between 30 s to hundreds of milliseconds, and stable NSs, which resist collapse completely (Kasen, Fernández & Metzger

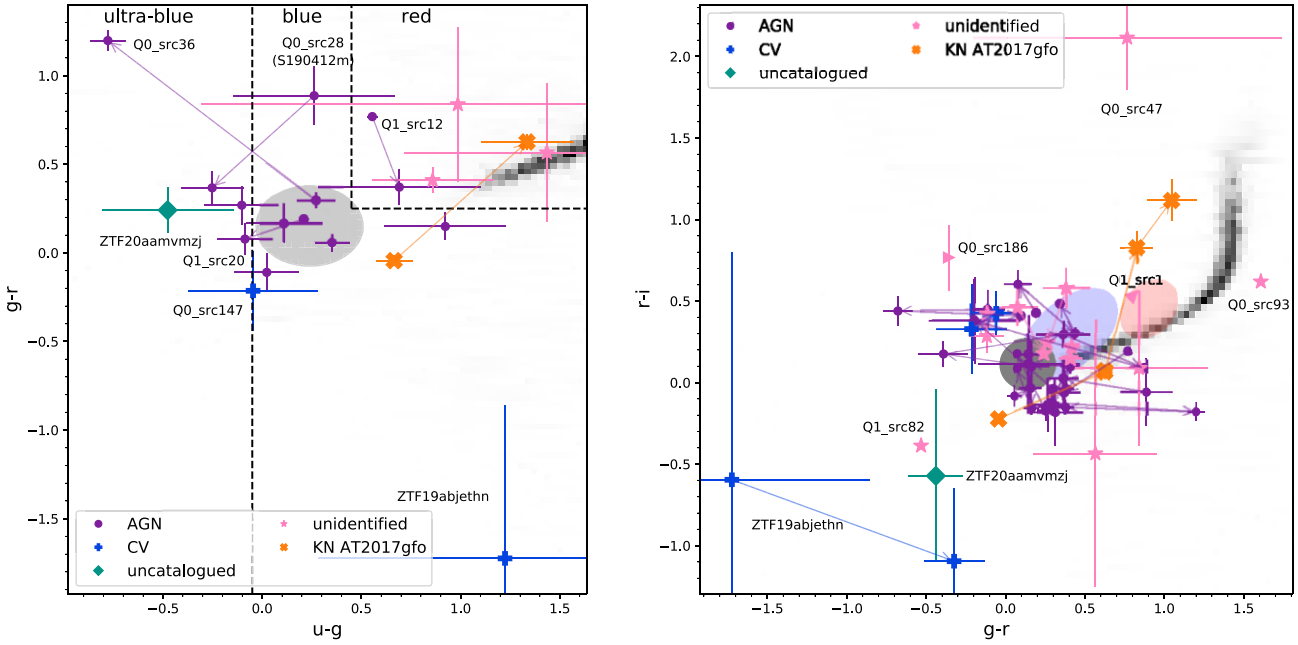

Figure 6. Colour–colour diagram of the archival photometry of the sources of interest, separated into the five initial categories (see legend), with photometry taken from the SDSS, CFHTLS, the Pan-STARRS stacked exposures, and DES catalogues. Left: $u-g$ versus $g-r$. Right: $g-r$ versus $r-i$. In the left-hand panel, the dotted lines divide the figure into regions identifying objects as red, blue, and ultra-blue, adapted from Lawrence et al. (2016). In both panels, the grey region indicates the colour location of 90 per cent of SDSS spectroscopic quasars (see Lawrence et al. 2016, for details), and we display a 2D histogram, given in grey, of the SDSS colours of 10 000 stars from the *Gaia* DR2 catalogue, selected from a region at high Galactic latitude. In the right-hand panel, the blue region represents the location of the blue cloud galaxies, and the red region represents the red-sequence galaxies, both out to $z = 0.22$ (adapted from Lawrence et al. 2016). In each panel, arrows connect points of the same source in chronological order. In the left-hand panel, these are labelled. In both panels, we have labelled sources that are of particular interest as they are outliers compared to the majority of points. In both panels, we identify AT2017gfo, the EM counterpart to GW170817, in orange. In the right-hand panel, two sources have one filter with no detection, one in the g-band and the other in the r-band. These points have triangles pointing away from their limit. These colours have been corrected for Galactic extinction. We have not corrected for host extinction for those sources external to our Galaxy. Correction for host extinction would move points down and to the left in both panels.

2015; Margalit & Metzger 2019; Metzger 2019). It is expected that the most numerous remnants will be HMNS (Margalit & Metzger 2019; Metzger 2019), which are expected to produce blue emission. For BH–NS, the NS is expected to be swallowed whole, resulting in no/little observable emission (Shibata & Hotokezaka 2019) or if the NS is disrupted, the emission is expected to be predominantly red but possibly with some blue emission (Just et al. 2015; Metzger 2019). BH–NS mergers are expected to have higher dynamical ejecta mass compared to BNS mergers (Fernández & Metzger 2016; Metzger 2019) and thus the light curves are expected to be more luminous. However, on average BH–NS mergers are expected to be detected out to larger distances than BNS mergers (Abbott et al. 2020b), and so the benefit to an observer of the increase in luminosity may be more than offset by the larger expected source distance (Metzger 2019).

The blue emission can also provide more specific diagnostics, providing information on the geometry of the binary system, the emission mechanism, and the ejecta composition. For instance, a blue KN may be present only for a fraction of KNe, whereby the viewing angle is optimized (cf. Christie et al. 2019): for viewers close to the equatorial plane, the blue emission may be blocked by the high-opacity lanthanide-rich tidal ejecta (Kasen et al. 2015), whereas close to the binary rotation axis both blue and red parts of the KN may be observed. Several emission mechanisms can produce optical/UV emission in KNe, such as a form of wind produced by the accretion disc, neutrino driven or from the magnetized NS (Metzger et al. 2018), or the blue emission may be produced dynamically by the ejecta, by the tidal tail, or through shock heating of the ejecta. NS remnants with strong magnetic fields may also produce optical/UV emission that may be brighter than a radioactively powered KN (Metzger & Piro 2014; Metzger 2019; Fong et al. 2021). Therefore, additional observations of KNe in the blue are essential to understand the range of sources that can produce this emission (Metzger 2019). The early blue emission within the first hours may also be enhanced by heating caused by free neutrons in the outer mass layer of the ejecta (Metzger et al. 2015). It is therefore essential to obtain early, well-sampled multiwavelength observations of KNe in order to distinguish between the variations in behaviour due to differences in the merging system, properties of the in-going binary, and viewing angle relative to the binary inclination (Metzger 2019).

4.1.1 *Impact of UVOT on EM counterpart searches*

UVOT has many advantages over ground-based instrumentation in detecting and observing the optical/UV emission from KNe. *Swift* is the only satellite capable of performing a fast response targeted tiling campaign. Under optimal conditions, *Swift* may be re-pointed to begin tiled observations of the GW error region within an hour of detection. UVOT can observe 24 h a day and is not limited by the weather or a restricted viewing angle beyond that imposed by the Earth and the Sun. *Swift*/UVOT is, therefore, able to search for the EM counterpart to GW alerts in portions of the sky, which are restricted or of limited visibility to ground-based observers. Compared to the other facilities observing during O3 (e.g. Andreoni et al. 2019b; Goldstein et al. 2019; Lundquist et al. 2019; Ackley et al. 2020;

Andreoni et al. 2020; Antier et al. 2020; Gompertz et al. 2020; Kasliwal et al. 2020; Thakur et al. 2020; Vieira et al. 2020; Anand et al. 2021; Ohgami et al. 2021; Paterson et al. 2021), *Swift*/UVOT was consistently one of the fastest to commence observations of the GW error region and searches in a bluer band. Follow-up in blue filters was particularly advantageous for GW170817, whereby we caught the blue emission from AT2017gfo and were able to observe its evolution within the *u* and UV bands (Evans et al. 2017). With these advantages combined with improvements made to our observing strategy within the O3 period, under a repeat of the GW170817 scenario, we would have observed AT2017gfo 5 h before ground-based observatories (Tohuvavohu & Kennea 2017). Another advantage is that *Swift* provides simultaneous coverage of all UVOT fields in X-rays with the XRT. Therefore, for all UVOT sources of interest, e.g. the EM counterpart to the GW event or other sources of interest, we can immediately provide optical to X-ray ratios, providing an instantaneous snapshot of the multiband spectral behaviour. This is an advantage not afforded to any other facility performing regular EM follow-up of GW sources.

We have no strong evidence to identify any of the transients observed by UVOT in O3 as counterparts to the GW events, consistent with the reports by other IR/optical/UV facilities (Andreoni et al. 2019b; Goldstein et al. 2019; Lundquist et al. 2019; Ackley et al. 2020; Andreoni et al. 2020; Antier et al. 2020; Coughlin et al. 2020a, b; Gompertz et al. 2020; Kasliwal et al. 2020; Thakur et al. 2020; Vieira et al. 2020; Anand et al. 2021; Ohgami et al. 2021; Paterson et al. 2021). The localizations of the triggers are large (ranging from tens to thousands of square degrees). The observing strategy of *Swift* means that a maximum of 800 fields will be observed by UVOT for any given GW event, covering $\sim 68\,\mathrm{deg}^2$. In addition, the distances of the BNS merger events are typically a factor of 5 greater than that of GW170817 ($\sim$40 Mpc; Coulter et al. 2017), with BH–NS and BBH mergers typically at distances a factor of 10 greater than GW170817. For AT2017gfo, the EM counterpart of GW170817, the UVOT *u*-band magnitude was $18.19^{+0.09}_{-0.08}$ mag upon first detection, 15.3 h after the trigger and $19.00^{+0.17}_{-0.15}$ mag 1 d after the trigger. As the typical distance of BNS GW events in the O3 period is a factor of 5 times more distant, this would imply that the typical brightness in the *u*-band would be 3.3 magnitudes fainter than was observed for GW170817 (as discussed by Antier et al. 2020). Therefore, it is not surprising that UVOT did not detect an EM counterpart during O3 since the larger distances and localizations of the GW alerts make any potential EM counterpart harder to detect because a larger portion of the sky has to be searched, and any potential EM counterpart will be much fainter. However, it is worth noting that if an EM counterpart is observed earlier in its evolution, it may be brighter. In O3, *Swift* typically began searches for EM counterparts within 2–4 h after the trigger, 4–8 times earlier than the first UVOT exposure of AT2017gfo.

4.2 Serendipitous sources

During the follow-up by *Swift* of 18 GW events in the O3 period, 27 sources were found by UVOT that are classified as sources of interest. These sources were determined to have changed in magnitude at 3σ confidence compared with archival *u*- or *g*-band catalogued values. The date the catalogued entry was observed and the choice of catalogue is dependent on the source location on the sky and when these catalogues were produced. Therefore, these sources have been selected heterogeneously. During the O3 period, *Swift*/UVOT also followed up a further 13 sources reported by other facilities, which we also include in this discussion. Using catalogue information reported by VizieR, we divided these 40 sources into five initial classifications resulting in 11 candidate AGNs/QSOs, three CVs, nine SNe, 11 unidentified sources, and six uncatalogued sources. We will now explore these sources to try to confirm these classifications and to determine the progenitors of the unidentified and uncatalogued sources.

Of the candidate AGN, eight have some form of distance measurement (five photometric redshift, $\sim$0.05−3.7; three spectroscopic redshift, 0.7–1.5), which are typical of AGN distances (from $z \sim 0.01$ to $z > 7$; Zheng et al. 2004; Mazzucchelli et al. 2017). Of the nine candidate AGNs with archival SDSS observations, eight are classified morphologically as stars through the SDSS photometry suggesting that the photometry is dominated (at least at that epoch) by the AGN rather than the galaxy. Their light curves are the best sampled of all our sources. The light curves span several years and have low-level changes at small time-scales, and some have larger changes over several years (see Supplementary Figs S.1–S.3). The low-level changes are consistent with that expected for AGN, which is <1 mag and typically between 0 and 0.5 mag (MacLeod et al. 2012). This behaviour is consistent with that expected for AGN (Ulrich, Maraschi & Urry 1997), whereby the optical AGN temporal variability is often described as damped random walk (Kelly, Bechtold & Siemiginowska 2009). A few of the candidate AGN in our sample display larger changes in magnitude >1 mag over a decade or more in time. Similar behaviour was also identified by Lawrence et al. (2016) for a small number of blue transients. These transients showed extreme changes in brightness, with changes of >1.5 mag occurring over a decade in time. These were spectroscopically confirmed as AGN. Lawrence et al. (2016) hypothesized that these large-amplitude changes in brightness might be due to changes in accretion state or large-amplitude microlensing by stars in foreground galaxies. They note that AGNs with these extreme changes in brightness are rare of the order of 1 per 1000 or 10 000. This suggests that the candidate AGN in our sample with changes of >1 mag over a decade or more in time may also be 'hypervariable' AGN. Tidal disruption events (TDEs) may also cause a temporary increase in brightness over several months. With the limited information available and without spectroscopic identification, we cannot exclude the possibility that the increase in brightness of one or more of these candidate AGN may actually be due to a TDE. However, the likelihood of a TDE being observed in the UVOT field of view during O3 is minimal, with $<<0.1$ event expected within the entire UVOT O3 coverage (see Section 4.2.1).

Graham et al. (2020) suggested ZTF19abanrhr as a possible EM counterpart to GW190521 (c.f. Ashton et al. 2020; Palmese et al. 2021). This transient was associated with a flare of an AGN peaking around 50 d after the GW trigger. The light curve of this event before the GW event varied by only a few per cent, while the flare was a 5σ deviation from the baseline ZTF flux lasting around 50 d. There are four UVOT sources of interest, classified as candidate AGN, found during the follow-up of a GW event associated with a BBH merger: Q0_src10, Q0_src28, Q0_src36 (S190412m), and Q1_src40 (S200224ca). Of these sources, only Q1_src40 has a distance that could be consistent with that of the GW event. The light curve of this event, shown in Supplementary Fig. S.3, particularly around the time of the GW trigger, is not markedly different to the other candidate AGN displayed in the other panels. However, a flare associated with the BBH merger is likely to present only a few days to weeks after the GW (McKernan et al. 2019). Indeed, ZTF19abanrhr was first detected 34 d after the GW trigger (Graham et al. 2020). Since UVOT observations cease within a few days of the GW trigger, the brightening of an AGN associated with a GW event would likely be missed.

The 11 unidentified sources have light curves spanning similar duration as observed for the candidate AGN, although for most sources, there are fewer observations. These sources fall into three main clusters in Fig. 3. The first group includes Q1_src82 (S190718y); Q1_src49, Q1_src54, and Q1_src113 (S190814bv); and Q1_src56 from S200115j. These are slightly fainter but have a similar magnitude change as the candidate AGN in Fig. 3. On the $g-r$ versus $r-i$ colour panel of Fig. 6, Q1_src49, Q1_src54, and Q1_src113 (S190814bv) are consistent with the colours of the candidate AGN. The similarities in colour, brightness, and Δm suggest that these sources are also likely AGN. However, Q1_src82 is inconsistent with the candidate AGN colours. For Q1_src82, we note that in $g-r$ versus $r-i$ panel of Fig. 6, the archival magnitudes of this source are unusually blue compared to the rest of the sources and highlighted regions. This suggests that this source is not an AGN, but with the limited information available, we cannot constrain the origin of this source any further.

The second cluster of unidentified sources includes Q0_src186 (S190425z), Q0_src93 (S190930t), and Q0_src47 (S200224ca). They are all brighter and have a larger Δm compared to the candidate AGN and are positioned close to AT2017gfo, the EM counterpart to GW170817 in Fig. 3. Q0_src186 and Q0_src47 are similar in their properties. For Q0_src186, from UVOT observations, we measured a $\Delta m_u > 2.0$, but the source is not detected in stacked g-band Pan-STARRS exposures with limiting magnitude of this survey typically 23.3 mag. This suggests that Δm maybe >4.5 magnitudes. An estimate of the rate at which the source faded can be derived from the change in u-band magnitude, $\Delta m_u > 1.4$, between detection and the next UVOT exposure taken 27 h later. This gives a lower limit to the decay rate of 1.2 mag per day. For Q0_src47, from UVOT observations we measured $\Delta m_u > 2.2$. For this source, there are also g-band stacked images available in Pan-STARRS. The difference between this and the u-band initial detection suggests that the source changed in brightness by ∼5 mag. We can again estimate the rate of decay of this source by looking at the time and change in brightness between the UVOT detection and the next exposure. The change is $\Delta m_u > 1.4$ within 2.5 d. This implies a decline rate of >0.6 mag per day. The large decline rates of both Q0_src186 and Q0_src47 enable us to rule them out as slow-evolving transients such as SNe (Wheeler & Harkness 1990; Gal-Yam 2012), TDEs (van Velzen et al. 2021), and AGN (MacLeod et al. 2012; Smith et al. 2018), but we cannot exclude faster evolving transients such as GRBs (Sari, Piran & Narayan 1998), KNe (Metzger 2019), fast-evolving CVs and novae (e.g. Hachisu & Kato 2018), and flare stars (Osten et al. 2010; Schmidt et al. 2014). Archival observations of Q0_src47 and Q0_src186 by Pan-STARRS show point-like sources suggesting that the archival objects are stars or distant galaxies. For both sources, the photometry increases in brightness towards the red. Q0_src186 is not detected in g. Q0_src47 is at least two magnitudes fainter in g and r compared to i, z, and Y. In the $g-r$ versus $r-i$ colour panel of Fig. 6, the archival photometry of both Q0_src47 and Q0_src186 indicates that these are the reddest sources in $r-i$. A hypothesis of Q0_src186 being a flare of a red–brown dwarf was put forward by Lipunov et al. (2019). Q0_src93 is more peculiar. To date, it continues to be detected by UVOT but is decreasing in brightness. Archival observations by DES place this source as the reddest object on the $g-r$ versus $r-i$ colour plane, redder than galaxies and stars. A more thorough investigation of this source will be presented in Oates et al. (in preparation).

The third cluster of unidentified sources are Q1_src1, Q1_src39, and Q1_src62, all from S200115j. These sources lie in the top left of Fig. 3; they are faint but have $\Delta m_u > 4$. For Q1_src1, it is difficult to put meaningful constraints on the potential rate of decay of this source from UVOT observations since only two short exposures with limits consistent with the detection magnitude were taken after the initial UVOT detection, both within the first 24 h. UVOT took a third longer exposure but only 5 months later. This source was not detected in a short exposure taken 1.5 h before the initial detection, though the limit is only slightly deeper than the detection; this could suggest a rapid onset. However, in archival Pan-STARRS photometry, Q1_src1 shows a rapid change in i-band of 2 magnitudes on a time-scale of 20 min. For Q1_src39, we cannot give a very constraining decay rate either since there are 10 d between detection by UVOT and the subsequent exposure, but this event must have had a reasonably rapid onset since the change from an image taken 20 h prior is $\Delta m_u > 0.9$. For Q1_src62, it is also not possible to provide strong constraints on the onset or decay rate. The closest UVOT exposures to the UVOT detection exposure were taken 16 h before and 10 d after and have 3σ upper limits consistent with the detection magnitude. In the $g-r$ versus $r-i$ panel, we have only a lower limit to the redness of Q1_src1 since we have only an upper limit in r for this source, but it is one of the reddest sources in this panel. For Q1_src39 and Q1_src62, these two sources are among the reddest sources in $g-r$, though the errors are large. These sources are very faint in archival images, in Pan-STARRS for Q1_src1 and CFHTLS for Q1_src39 and Q1_src62, suggesting a faint star or distant galaxy origin. With the red archival values and the potentially rapid onset of Q1_src1 and Q1_src39, we suggest that Q1_src1, Q1_src39, and Q1_src62 could have similar nature as Q0_src47 (S200224ca) and Q0_src186 (S190425z).

We initially classified six of the sources of interest as uncatalogued. For these sources, there is no archival information providing an identification, and for only one, we were able to produce a light curve: ZTF20aamvmzj, shown in Supplementary Fig. S.7. In this figure, we display data obtained by both UVOT and Kasliwal et al. (2020). Blue evolution is observed, with the UV filters declining while the ZTF g-band and r-band remain constant. Power-law fits also confirm this, which give $\alpha = 0.04$ in the r-band (Kasliwal et al. 2020) and -1.45 ± 0.23 measured from the combined UVOT data. ZTF20aamvmzj displays behaviour reminiscent of Type II SNe. In Supplementary Fig. S.7, we overlay the optical/UV light curves of ASASSN-14ha (Valenti et al. 2016), which were obtained from the Open Supernova Catalog (Guillochon et al. 2017). We scaled the light curves of ASASSN-14ha by six magnitudes, corresponding to a factor of ≈16 in distance. The similarities in light-curve evolution between ZTF20aamvmzj and ASASSN-14ha suggest that ZTF20aamvmzj is most likely a Type II SN at a distance of ∼350 Mpc.

For Cand-A09, we cannot draw any conclusion as to the rate of decay of this object since the second UVOT image was taken 2 yr after the initial detection. However, we note that in Fig. 3, this source lies just beneath the CV cluster and only a lower limit is known on Δm. Therefore, it is possible that this source is a CV.

For the remaining four uncatalogued sources, Q0_src136 (S190425z), Q1_src33 (S190930t), Q1_src58 (S200115j), and Q1_src54 (S200224ca), we re-examined the UVOT images to ensure that these sources were not due to scattered light. If these were ghosts, we would expect a bright source in the FOV. However, no bright sources are apparent in any of the images. The full-frame image and zoom-in on the source location for each of these objects are provided in Supplementary Fig. S.8. In Fig. 3, three of these sources have peak magnitudes slightly brighter than that found for most of the candidate AGNs and the unidentified sources, and Δm for these three sources is $\gtrsim 1$ mag. The first image taken after the initial UVOT detection for two of these sources, Q0_src136 (S190425z) and

Q1_src54 (S200224ca), was over 2 months later, so we cannot draw useful constraints on the decay rate or hence draw further conclusions on the nature of these two sources. Q1_src54 does, however, have a WISE source within 4 arcsec, which may indicate an underlying red object. Interestingly, for Q1_src58, we have a detection at a magnitude of 21.31 ± 0.37 lasting 486 s and then another 476 exposure starting just 48 s after the first exposure giving a 3σ upper limit (>21.22). However, for this source and Q1_src33 (S190930t), the detection and upper limit measured in the subsequent exposure are consistent, so we cannot draw firm conclusions. We suggest that these four uncatalogued UVOT sources could be similar to Q0_src47 (S200224ca) and Q0_src186 (S190425z). We base this assumption on the lack of archival detections and because these sources were detected in a single UVOT exposure, similar to Q1_src1, Q1_src39, and Q1_src62 (S200115j).

4.2.1 Transient density in UVOT

Within the 424 deg^2 observed at least once by UVOT during the O3 period, UVOT found 27 transient sources. These were deemed to be transient based on their increase in brightness at 3σ confidence compared with archival *u*- or *g*-band catalogued magnitudes. This provides a detection surface density of transient sources brighter than 21.2 mag of 0.064 deg^{-2} in the *u* filter. Of the 27 sources, we initially identified 10 as candidate AGNs, and five unidentified sources are also likely to be AGNs, bringing the total of candidate AGNs to 15. The rate of AGN with transient behaviour found by the UVOT during the O3 period is therefore 0.024–0.035 deg^{-2} in the *u* filter. Similarly, we estimate that between five and nine of the UVOT sources of interest are fast-evolving transients, which are red sources in quiescence, e.g. Q0_src47 (S200224ca) and Q0_src186 (S190425z), one possibility is that these are flare stars. The transient density for these sources is 0.012–0.021 deg^{-2} in the *u* filter. We did not conclusively detect any TDE candidates. The TDE rate brighter than ∼21 mag is 1 per month (van Velzen et al. 2020), assuming a duration of 6 months, there should be a few TDEs on the sky at any time. With the UVOT sky coverage of 424 deg^2 during O3, we, therefore, expect a rate of a few ×0.01 TDEs within the O3 coverage. This is consistent with zero-confirmed TDEs observed by UVOT.

4.3 Future improvements to GW follow-up by UVOT

Swift/UVOT was essential to the discovery of blue emission produced by the KN associated with 170817 (Evans et al. 2017). Through the rapid planning capabilities devised by the *Swift* team (Tohuvavohu & Kennea 2017), the typical start time of *Swift* tiling is 2–4 h after the trigger, with observations commencing as early as 1.8 h for S200114f. This rapid capability combined with the relatively unrestricted observing windows and the blue coverage of the UVOT is important for detecting the KN and observing its early evolution (Metzger et al. 2015; Metzger 2019). With the advantages *Swift* has over ground-based facilities, the *Swift* team is continually endeavouring to optimize the search of the LVC error regions.

One of the greatest drawbacks UVOT currently has is the identification of new sources within galaxies. The majority of thumbnails produced by the UVOT pipeline are marked as 'gal'. Currently, these galaxy images are manually scrutinized for changes in brightness or any new point sources by comparing with the archival UVOT image, if available, or the DSS image. However, the capacity to find transients this way is limited. We do not have archival UVOT images for most of these galaxies. Therefore, a visual inspection and comparison to DSS images in the blue band can easily miss small changes in brightness and perhaps even large changes if the galaxy core is overexposed in the DSS. One of the improvements that attempts to address this will be the completion of the SGWGS catalogue (as discussed in Section 2.1.3; Tohuvavohu et al., in preparation), which is expected to observe a total of 13 000 galaxies. Having a template UVOT, *u*-band image to directly compare against a GW *u*-band tile should mitigate some of the issues of comparing against archival images from other facilities. These *u*-band images and other archival UVOT *u*-band images will be used during side-by-side (or blinked) comparison with the tiled GW images, and we shall explore whether image subtraction improves the identification of the transient source and, if successful, implement this in the UVOT pipeline.

With experience gained during O3, we are currently looking at how we can improve the UVOT pipeline and manual checking procedures in the run-up to O4 to optimize the possibility of finding an EM counterpart in the optical/UV. We will expand the UVOT pipeline to automatically create light curves for all Q0, Q1, Q2, and Q3 sources, using UV/optical/IR catalogues and photometry available through VizieR, IRSA, and other sources. The pipeline will automatically report the listing of sources in astronomical catalogues as potential AGN, RR lyre stars etc. Using archival information, we will be able to quickly check the position of the source on colour–colour diagrams such as the $g-r$ versus $r-i$ in Fig. 6, in order to prioritize follow-up for those UVOT transients. In particular, UV transients consistent with residing in elliptical galaxies may be worth prioritizing since, according to Fig. 6, UV transients appear to be relatively rare in elliptical galaxies. There is some chance that short GRBs may be hosted in elliptical galaxies. All of this will enable rapid identification of sources, identify whether they are known objects, and will initiate rapid follow-up to determine if the source is a candidate EM counterpart of the GW event or another source of interest that should be explored further.

In addition, for around 10 per cent of tiles observed by *Swift*, UVOT uses a less sensitive filter (e.g. *uvw1*) or a blocked filter so that damage to the UVOT is avoided due to bright stars/fields. This means that for every GW event observed by *Swift*/UVOT, there are a non-negligible number of potential host galaxies that cannot be observed. In the run-up to O4, we will explore whether we can adapt the field selection algorithm to offset the pointing, where possible, such that the bright star is avoided, but the potential host galaxy within a given tile is still observed.

5 CONCLUSION

In this paper, we summarized the *Swift*/UVOT pipeline and follow-up of GW events in the third LIGO–Virgo observing run, O3. During this cycle, *Swift*/UVOT GW followed up 18 GW events to differing extents. Using the classifications issued by LVC and reported in the GraceDB, these events can be categorized as five BBH mergers, six BNS mergers (three of which had a larger probability of being terrestrial rather than BNS), three BH–NS, two mass-gap triggers, and two unmodelled/burst triggers. Of these, three were quickly retracted: one BNS, one BH–NS, and one unmodelled, and three were not included in the GWTC-2 catalogue of O3a: two BNS and one BH–NS. Across all 18 GW events, *Swift*/UVOT observed 6441 individual fields (tiles). All images were processed through the UVOT GW pipeline, which identifies sources of interest and gives them a quality flag. All sources identified are manually verified. Sources deemed more likely to be actual transients are assigned a flag of 0 (referred to as Q0 sources) or 1 depending on their magnitude.

Sources dimmer than a magnitude of 19.9 (a conservative sensitivity limit to obtain a signal to noise >5 in the ∼80 s tiling observations) are assigned a value of 1. The automatic analysis pipeline found a total of 1516 Q0 and Q1 sources to be verified.

After manual inspection, 27 sources were considered to be of interest. These sources were determined to have changed in magnitude at 3σ confidence compared with archival *u*- or *g*-band catalogued values. *Swift*/UVOT also followed up a further 13 sources reported by other facilities during the O3 period. Using catalogue information reported by VizieR, we divided these 40 sources into five initial classifications: 11 candidate AGNs/QSOs; three cataclysmic variables; nine supernovae; 11 unidentified sources with archival photometry but no classification; and six uncatalogued sources for which no archival photometry was available. We further examined these sources of interest to determine if we could classify the unidentified and uncatalogued sources. For this analysis, we examined and compared the information available from all 40 sources. We find it likely that most of the unidentified and uncatalogued sources are AGN, a class of fast-evolving transient and one source may be a CV. We have no substantial evidence to identify any of these transients as counterparts to the GW events.

Finally, we suggested improvements that can be made to the UVOT pipeline and manual verification of sources before the start of the LIGO–Virgo–KAGRA O4 run. One of the most significant improvements will be incorporating archival UVOT images into the pipeline for comparison with UVOT images taken during the O4 run, likely commencing mid-2022. In particular, we will be including 13 000 images from the SGWGS catalogue, a catalogue of *u*-band images of nearby galaxies. UVOT is a crucial instrument in the detection and follow-up of blue emission associated with GW events. *Swift*'s unique capabilities place it in a prime position to detect the EM counterpart to a GW early on and to provide the astronomical community with coverage of large portions of the GW error region that may otherwise be constrained or have delayed observations from ground-based telescopes. The current estimated re-entry time of *Swift* is around 2035, providing funding is continued; this suggests that UVOT has many more successful years ahead chasing EM counterparts to GWs as well as remaining the workhorse of the transient community.

ACKNOWLEDGEMENTS

We thank the referee and M. Nicholl for useful discussion and suggestions that improved the paper. This research has made use of data obtained from the High Energy Astrophysics Science Archive Research Center (HEASARC) and the Leicester Database and Archive Service (LEDAS), provided by NASA's Goddard Space Flight Center and the School of Physics and Astronomy, University of Leicester, UK, respectively. This research has also made use of a number of public services: the VizieR catalogue access tool, CDS, Strasbourg, France (DOI: 10.26093/cds/vizier); the International Astronomical Union Minor Planet Center, which is hosted by the Center for Astrophysics at the Harvard & Smithsonian and is funded by NASA; and data from the European Space Agency (ESA) mission *Gaia* (https://www.cosmos.esa.int/gaia), processed by the *Gaia* Data Processing and Analysis Consortium (DPAC, https://www.cosmos.esa.int/web/gaia/dpac/consortium). The CSS survey is funded by the National Aeronautics and Space Administration under grant no. NNG05GF22G issued through the Science Mission Directorate Near-Earth Objects Observations Program. The CRTS survey is supported by the U.S. National Science Foundation under grants AST-0909182 and AST-1313422. This publication makes use of data products from the Wide-field Infrared Survey Explorer, which is a joint project of the University of California, Los Angeles, and the Jet Propulsion Laboratory/California Institute of Technology, funded by the National Aeronautics and Space Administration. The CFHTLS data are based on observations obtained with MegaPrime/MegaCam, a joint project of CFHT and CEA/IRFU, at the Canada–France–Hawaii Telescope (CFHT), which is operated by the National Research Council (NRC) of Canada, the Institut National des Science de l'Univers of the Centre National de la Recherche Scientifique (CNRS) of France, and the University of Hawaii. This work is based in part on data products produced at Terapix available at the Canadian Astronomy Data Centre as part of the Canada–France–Hawaii Telescope Legacy Survey, a collaborative project of NRC and CNRS. This research has made use of the NASA/IPAC Infrared Science Archive, which is funded by the National Aeronautics and Space Administration and operated by the California Institute of Technology. The Pan-STARRS1 Surveys (PS1) and the PS1 public science archive have been made possible through contributions by the Institute for Astronomy, the University of Hawaii, the Pan-STARRS Project Office, the Max-Planck Society and its participating institutes, the Max-Planck Institute for Astronomy, Heidelberg, the Max-Planck Institute for Extraterrestrial Physics, Garching, The Johns Hopkins University, Durham University, the University of Edinburgh, the Queen's University Belfast, the Harvard-Smithsonian Center for Astrophysics, the Las Cumbres Observatory Global Telescope Network Incorporated, the National Central University of Taiwan, the Space Telescope Science Institute, the National Aeronautics and Space Administration under grant no. NNX08AR22G issued through the Planetary Science Division of the NASA Science Mission Directorate, the National Science Foundation grant no. AST-1238877, the University of Maryland, Eotvos Lorand University (ELTE), the Los Alamos National Laboratory, and the Gordon and Betty Moore Foundation. SRO gratefully acknowledges the support of the Leverhulme Trust Early Career Fellowship. AAB, NPMK, MJP, KLP, PAE, APB, and JPO acknowledge funding from the UK Space Agency. MDP acknowledges support for this work by the Scientific and Technological Research Council of Turkey (TÜBITAK), grant no: MFAG-119F073. EA, MGB, SC, GC, AD, PDA, AM, and GT acknowledge funding from the Italian Space Agency, contract ASI/INAF n. I/004/11/4. This work is also partially supported by a grant from the Italian Ministry of Foreign Affairs and International Cooperation Nr. MAE0065741. PDA acknowledges support from PRIN-MIUR 2017 (grant 20179ZF5KS). DBM is supported by research grant 19054 from Villum Fonden.

DATA AVAILABILITY

The data underlying this article are available in the *Swift* archives at https://www.swift.ac.uk/swift_live/, https://heasarc.gsfc.nasa.gov/cgi-bin/W3Browse/swift.pl, https://www.ssdc.asi.it/mmia/index.php?mission = swiftmastr, and in the online supplementary material.

REFERENCES

Aasi J. et al., 2015, Class. Quantum Gravity, 32, 115012
Abbott B. P. et al., 2009, Rep. Prog. Phys., 72, 076901
Abbott B. P. et al., 2017a, ApJ, 848, L13
Abbott B. P. et al., 2017b, ApJ, 848, L12
Abbott B. P. et al., 2017c, Nature, 551, 85
Abbott B. P. et al., 2020a, ApJ, 892, L3
Abbott B. P. et al., 2020b, Living Rev. Relativ., 23, 3

Abbott R. et al., 2020c, Phys. Rev., 11, 021053
Abbott R. et al., 2020d, Phys. Rev. Lett., 125, 101102
Abbott R. et al., 2020e, ApJ, 896, L44
Abbott T. M. C. et al., 2018, ApJS, 239, 18
Acernese F. et al., 2015, Class. Quantum Gravity, 32, 024001
Ackley K. et al., 2020, A&A, 643, A113
Alam S. et al., 2015, ApJS, 219, 12
Alexander K. D. et al., 2018, ApJ, 863, L18
Anand S. et al., 2021, Nature Astron., 5, 46
Andreoni I. et al., 2017, Publs. Astr. Soc. Australia, 34, e069
Andreoni I. et al., 2019a, GCN Circ., 26424, 1
Andreoni I. et al., 2019b, ApJ, 881, L16
Andreoni I. et al., 2020, ApJ, 890, 131
Antier S. et al., 2020, MNRAS, 497, 5518
Arcavi I. et al., 2017, Nature, 551, 64
Ashton G., Ackley K., Magaña Hernandez I., Piotrzkowski B., 2020, preprint (arXiv:2009.12346)
Assef R. J., Stern D., Noirot G., Jun H. D., Cutri R. M., Eisenhardt P. R. M., 2018, ApJS, 234, 23
Barnes J., Kasen D., 2013, ApJ, 775, 18
Barthelmy S. D. et al., 2005, Space Sci. Rev., 120, 143
Bellm E. C. et al., 2019, PASP, 131, 018002
Bertin E., Arnouts S., 1996, A&AS, 117, 393
Bianchi L., Conti A., Shiao B., 2014, Adv. Space Res., 53, 900
Bilicki M., Jarrett T. H., Peacock J. A., Cluver M. E., Steward L., 2014, ApJS, 210, 9
Breeveld A. A., Landsman W., Holland S. T., Roming P., Kuin N. P. M., Page M. J., 2011, in McEnery J. E., Racusin J. L., Gehrels N., eds, AIP Conf. Proc. Vol. 1358, Gamma Ray Bursts 2010. Am. Inst. Phys., New York, 373
Burrows D. N. et al., 2005, Space Sci. Rev., 120, 165
Burrows D. N. et al., 2006, ApJ, 653, 468
Cantiello M. et al., 2018, ApJ, 854, L31
Chambers K. C. et al., 2016, preprint (arXiv:1612.05560)
Chornock R. et al., 2017, ApJ, 848, L19
Christie I. M., Lalakos A., Tchekhovskoy A., Fernández R., Foucart F., Quataert E., Kasen D., 2019, MNRAS, 490, 4811
Coughlin M. W. et al., 2020a, MNRAS, 497, 1181
Coughlin M. W. et al., 2020b, MNRAS, 492, 863
Coulter D. A. et al., 2017, Science, 358, 1556
Cowperthwaite P. S. et al., 2017, ApJ, 848, L17
Cuillandre J.-C. J. et al., 2012, in Adler D. S., Seaman R. L., Benn C. R., eds, Proc. SPIE Conf. Ser. Vol. 8448, Observatory Operations: Strategies, Processes, and Systems IV. SPIE, Bellingham, p. 84480M
Cutri R. M. et al., 2021, VizieR Online Data Catalog, II/328
Dálya G. et al., 2018, MNRAS, 479, 2374
Díaz M. C. et al., 2017, ApJ, 848, L29
Dichiara S., Troja E., O'Connor B., Marshall F. E., Beniamini P., Cannizzo J. K., Lien A. Y., Sakamoto T., 2020, MNRAS, 492, 5011
Dobie D. et al., 2019, ApJ, 887, L13
Drake A. J. et al., 2009, ApJ, 696, 870
Drout M. R. et al., 2017, Science, 358, 1570
Eichler D., Livio M., Piran T., Schramm D. N., 1989, Nature, 340, 126
Evans P. A. et al., 2016a, MNRAS, 460, L40
Evans P. A. et al., 2016b, MNRAS, 462, 1591
Evans P. A. et al., 2017, Science, 358, 1565
Evans P. A. et al., 2019a, MNRAS, 484, 2362
Evans P. A. et al., 2019b, GCN Circ., 26498, 1
Fernández R., Metzger B. D., 2016, Annu. Rev. Nucl. Part. Sci., 66, 23
Fong W. et al., 2013, ApJ, 769, 56
Fong W., Berger E., Margutti R., Zauderer B. A., 2015, ApJ, 815, 102
Fong W. et al., 2017, ApJ, 848, L23
Fong W. et al., 2019, ApJ, 883, L1
Fong W. et al., 2021, ApJ, 906, 127
Gaia Collaboration 2018, A&A, 616, A1
Gal-Yam A., 2012, Science, 337, 927
Gall C., Hjorth J., Rosswog S., Tanvir N. R., Levan A. J., 2017, ApJ, 849, L19
Gehrels N. et al., 2004, Astrophys. J., 611, 1005
Gehrels N. et al., 2005, Nature, 437, 851
Ghirlanda G. et al., 2019, Science, 363, 968
Goldstein A. et al., 2017, ApJ, 848, L14
Goldstein D. A. et al., 2019, ApJ, 881, L7
Gomez S. et al., 2019, ApJ, 884, L55
Gompertz B. P. et al., 2020, MNRAS, 497, 726
Graham M. J. et al., 2019, PASP, 131, 078001
Graham M. J. et al., 2020, Phys. Rev. Lett., 124, 251102
Guidorzi C. et al., 2017, ApJ, 851, L36
Guillochon J., Parrent J., Kelley L. Z., Margutti R., 2017, ApJ, 835, 64
Hachisu I., Kato M., 2018, ApJS, 237, 4
Haggard D., Nynka M., Ruan J. J., Kalogera V., Cenko S. B., Evans P., Kennea J. A., 2017, ApJ, 848, L25
Hajela A. et al., 2019, ApJ, 886, L17
Hallinan G. et al., 2017, Science, 358, 1579
HAWC Collaboration, 2019, GCN Circ., 26472, 1
Hotokezaka K., Nakar E., Gottlieb O., Nissanke S., Masuda K., Hallinan G., Mooley K. P., Deller A. T., 2019, Nature Astron., 3, 940
Hu L. et al., 2017, Sci. Bull., 62, 1433
Hussain R., 2019, GCN Circ., 26463, 1
IceCube Collaboration, 2019, GCN Circ., 26460, 1
IceCube Collaboration, 2020, GCN Circ., 27043, 1
Jin Z.-P. et al., 2018, ApJ, 857, 128
Just O., Bauswein A., Ardevol Pulpillo R., Goriely S., Janka H. T., 2015, MNRAS, 448, 541
Kagra Collaboration, 2019, Nature Astron., 3, 35
Kasen D., Fernández R., Metzger B. D., 2015, MNRAS, 450, 1777
Kasliwal M. M. et al., 2017, Science, 358, 1559
Kasliwal M. M. et al., 2019, GCN Circ., 24191, 1
Kasliwal M. M. et al., 2020, ApJ, 905, 145
Kasliwal M. M., Collaboration ZTF, Collaboration GROWTH, 2020, GCN Circ., 27051, 1
Kawaguchi K., Shibata M., Tanaka M., 2020, ApJ, 889, 171
Kelly B. C., Bechtold J., Siemiginowska A., 2009, ApJ, 698, 895
Klingler N. J. et al., 2019, ApJS, 245, 15
Klingler N. J. et al., 2021, ApJ, 907, 97
Korobkin O. et al., 2021, ApJ, 910, 116
Kuin N. P. M., Swift Team, 2019, GCN Circ., 24863, 1
Laha S., Gronwall C., Klingler N. J., Lien A. Y., Page K. L., Tohuvavohu A., Neil Gehrels Swift Observatory Team, 2020, GCN Circ., 27234, 1
Lamb G. P. et al., 2019, ApJ, 870, L15
Lasker B. M. et al., 2008, AJ, 136, 735
Lattimer J. M., Schramm D. N., 1974, ApJ, 192, L145
Law N. M. et al., 2009, PASP, 121, 1395
Lawrence A. et al., 2016, MNRAS, 463, 296
Lee M. G., Kang J., Im M., 2018, ApJ, 859, L6
LIGO Scientific Collaboration, Virgo Collaboration, 2019a, GCN Circ., 24098, 1
LIGO Scientific Collaboration, Virgo Collaboration, 2019b, GCN Circ., 24168, 1
LIGO Scientific Collaboration, Virgo Collaboration, 2019c, GCN Circ., 24237, 1
LIGO Scientific Collaboration, Virgo Collaboration, 2019d, GCN Circ., 25549, 1
LIGO Scientific Collaboration, Virgo Collaboration, 2019e, GCN Circ., 24442, 1
LIGO Scientific Collaboration, Virgo Collaboration, 2019f, GCN Circ., 24489, 1
LIGO Scientific Collaboration, Virgo Collaboration, 2019g, GCN Circ., 25087, 1
LIGO Scientific Collaboration, Virgo Collaboration, 2019h, GCN Circ., 25187, 1
LIGO Scientific Collaboration, Virgo Collaboration, 2019i, GCN Circ., 25296, 1
LIGO Scientific Collaboration, Virgo Collaboration, 2019j, GCN Circ., 25324, 1

LIGO Scientific Collaboration, Virgo Collaboration, 2019k, GCN Circ., 25333, 1
LIGO Scientific Collaboration, Virgo Collaboration, 2019l, GCN Circ., 25876, 1
LIGO Scientific Collaboration, Virgo Collaboration, 2019m, GCN Circ., 26222, 1
LIGO Scientific Collaboration, Virgo Collaboration, 2019n, GCN Circ., 26250, 1
LIGO Scientific Collaboration, Virgo Collaboration, 2019o, GCN Circ., 26402, 1
LIGO Scientific Collaboration, Virgo Collaboration, 2019p, GCN Circ., 26454, 1
LIGO Scientific Collaboration, Virgo Collaboration, 2019q, GCN Circ., 26570, 1
LIGO Scientific Collaboration, Virgo Collaboration, 2019r, GCN Circ., 25301, 1
LIGO Scientific Collaboration, Virgo Collaboration, 2020a, GCN Circ., 26734, 1
LIGO Scientific Collaboration, Virgo Collaboration, 2020b, GCN Circ., 26759, 1
LIGO Scientific Collaboration, Virgo Collaboration, 2020c, GCN Circ., 27042, 1
LIGO Scientific Collaboration, Virgo Collaboration, 2020d, GCN Circ., 27184, 1
LIGO Scientific Collaboration, Virgo Collaboration, 2020e, GCN Circ., 27193, 1
Li L.-X., Paczyński B., 1998, ApJ, 507, L59
Lippuner J., Fernández R., Roberts L. F., Foucart F., Kasen D., Metzger B. D., Ott C. D., 2017, MNRAS, 472, 904
Lipunov V. M. et al., 2017, ApJ, 850, L1
Lipunov V. et al., 2019, GCN Circ., 24326, 1
Lundquist M. J. et al., 2019, ApJ, 881, L26
Lyman J. D. et al., 2018, Nature Astron., 2, 751
Lynch R., Vitale S., Essick R., Katsavounidis E., Robinet F., 2017, Phys. Rev. D, 95, 104046
MacLeod C. L. et al., 2012, ApJ, 753, 106
Margalit B., Metzger B. D., 2019, ApJ, 880, L15
Margutti R. et al., 2017, ApJ, 848, L20
Mazzucchelli C. et al., 2017, ApJ, 849, 91
McBrien O. et al., 2019, GCN Circ., 26485, 1
McCully C. et al., 2017, ApJ, 848, L32
McKernan B. et al., 2019, ApJ, 884, L50
Metzger B. D., 2017, Living Rev. Relativ., 20, 3
Metzger B. D., 2019, Living Rev. Relativ., 23, 1
Metzger B. D., Fernández R., 2014, MNRAS, 441, 3444
Metzger B. D., Piro A. L., 2014, MNRAS, 439, 3916
Metzger B. D. et al., 2010, MNRAS, 406, 2650
Metzger B. D., Bauswein A., Goriely S., Kasen D., 2015, MNRAS, 446, 1115
Metzger B. D., Thompson T. A., Quataert E., 2018, ApJ, 856, 101
Monet D. G. et al., 2003, AJ, 125, 984
Mooley K. P. et al., 2018, Nature, 554, 207
Narayan R., Paczynski B., Piran T., 1992, ApJ, 395, L83
Nicholl M. et al., 2017, ApJ, 848, L18
Ochsenbein F., Bauer P., Marcout J., 2000, A&AS, 143, 23
Ohgami T. et al., 2021, PASJ, 73, 350
Osten R. A. et al., 2010, ApJ, 721, 785
Page M. J. et al., 2014, in Proceedings of Swift: 10 Years of Discovery (SWIFT 10). SISSA, Trieste, p. 37
Page K. L. et al., 2020, MNRAS, 499, 3459
Palmese A. et al., 2017, ApJ, 849, L34
Palmese A., Fishbach M., Burke C. J., Annis J. T., Liu X., 2021, ApJ, 914, L34
Paterson K. et al., 2021, ApJ, 912, 128
Perego A., Rosswog S., Cabezón R. M., Korobkin O., Käppeli R., Arcones A., Liebendörfer M., 2014, MNRAS, 443, 3134
Perley D. A. et al., 2019, GCN Circ., 24331, 1
Perna R., Lazzati D., Farr W., 2019, ApJ, 875, 49
Pian E. et al., 2017, Nature, 551, 67
Poole T. S. et al., 2008, Mon. Not. R. Astr. Soc., 383, 627
Pozanenko A. S. et al., 2018, ApJ, 852, L30
Reusch S., Stein R., Perley D., Anand S., Zwicky Transient Facility (ZTF) Collaboration, Global Relay of Observatories Watching Transients Happen (Growth) Collaboration, 2020, GCN Circ., 27068, 1
Roming P. W. A. et al., 2005, Space Sci. Rev., 120, 95
Rosswog S., Korobkin O., Arcones A., Thielemann F. K., Piran T., 2014, MNRAS, 439, 744
Sari R., Piran T., Narayan R., 1998, ApJ, 497, L17
Savchenko V. et al., 2017, ApJ, 848, L15
Schmidt S. J. et al., 2014, ApJ, 781, L24
Shappee B. J. et al., 2017, Science, 358, 1574
Shibata M., Hotokezaka K., 2019, Annu. Rev. Nucl. Part. Sci., 69, 41
Singer L. et al., 2019, GCN Circ., 26479, 1
Smartt S. J. et al., 2017, Nature, 551, 75
Smith K. L., Mushotzky R. F., Boyd P. T., Malkan M., Howell S. B., Gelino D. M., 2018, ApJ, 857, 141
Smith K. W. et al., 2019, GCN Circ., 24210, 1
Soares-Santos M. et al., 2017, ApJ, 848, L16
Stein R. et al., 2019a, GCN Circ., 25899, 1
Stein R., Reusch S., Perley D., Andreoni I., Coughlin M., Zwicky Transient Facility Collaboration, Global Relay of Transients Watching Observatories Happen Collaboration, 2019b, GCN Circ., 26437, 1
Stewart A. et al., 2019, GCN Circ., 25487, 1
Tanvir N. R. et al., 2017, ApJ, 848, L27
Thakur A. L. et al., 2020, MNRAS, 499, 3868
The LIGO Scientific Collaboration, the Virgo Collaboration, 2019, GCN Circ., 24045, 1
The LIGO Scientific Collaboration, 2020, preprint (arXiv:2004.08342)
Tohuvavohu A., Kennea J. A., 2017, preprint (arXiv:1712.07058)
Tohuvavohu A., Kennea J. A., DeLaunay J., Palmer D. M., Cenko S. B., Barthelmy S., 2020, ApJ, 900, 35
Troja E. et al., 2016, ApJ, 827, 102
Troja E. et al., 2017, Nature, 551, 71
Troja E. et al., 2019, MNRAS, 489, 1919
Troja E. et al., 2020, MNRAS, 498, 5643
Ulrich M.-H., Maraschi L., Urry C. M., 1997, Ann. Rev. Astron. Astrophys., 35, 445
Utsumi Y. et al., 2017, PASJ, 69, 101
Valenti S. et al., 2016, MNRAS, 459, 3939
Valenti S. et al., 2017, ApJ, 848, L24
van Velzen S., Holoien T. W. S., Onori F., Hung T., Arcavi I., 2020, Space Sci. Rev., 216, 124
van Velzen S. et al., 2021, ApJ, 908, 4
Vieira N. et al., 2020, ApJ, 895, 96
Villar V. A. et al., 2017, ApJ, 851, L21
Villar V. A. et al., 2018, ApJ, 862, L11
Webb N. A. et al., 2020, A&A, 641, A136
Wheeler J. C., Harkness R. P., 1990, Rep. Prog. Phys., 53, 1467
White D. J., Daw E. J., Dhillon V. S., 2011, Class. Quantum Gravity, 28, 085016
Wollaeger R. T. et al., 2018, MNRAS, 478, 3298
Wright E. L. et al., 2010, AJ, 140, 1868
Wyatt S. D., Tohuvavohu A., Arcavi I., Lundquist M. J., Howell D. A., Sand D. J., 2020, ApJ, 894, 127
Zheng W. et al., 2004, ApJS, 155, 73

SUPPORTING INFORMATION

Supplementary data are available at *MNRAS* online.

Swift_UVOT_GW_O3_Supplementary_Material.pdf

Please note: Oxford University Press is not responsible for the content or functionality of any supporting materials supplied by the authors.

Any queries (other than missing material) should be directed to the corresponding author for the article.

[1]*School of Physics and Astronomy & Institute for Gravitational Wave Astronomy, University of Birmingham, Birmingham B15 2TT, UK*
[2]*University College London, Mullard Space Science Laboratory, Holmbury St. Mary, Dorking RH5 6NT, UK*
[3]*Department of Physics, University of Warwick, Coventry CV4 7AL, UK*
[4]*Astrophysics Science Division, NASA Goddard Space Flight Center, Greenbelt, MD 20771, USA*
[5]*George P. and Cynthia Woods Mitchell Institute for Fundamental Physics and Astronomy, Mitchell Physics Building, Texas A.&M. University, Department of Physics and Astronomy, College Station, TX 77843, USA*
[6]*Department of Astronomy and Space Sciences, Istanbul University, Beyazıt, 34119, Istanbul, Turkey*
[7]*School of Physics and Astronomy, University of Leicester, Leicester LE1 7RH, UK*
[8]*Department of Astronomy and Astrophysics, The Pennsylvania State University, University Park, PA 16802, USA*
[9]*Institute for Gravitation and the Cosmos, The Pennsylvania State University, University Park, PA 16802, USA*
[10]*Department of Astronomy and Astrophysics, University of Toronto, Toronto, ON M5S 3H4, Canada*
[11]*INAF, IASF Palermo, Via Ugo La Malfa 153, I-90146, Palermo, Italy*
[12]*INAF, Osservatorio Astronomico di Brera, Via Bianchi 46, I-23807 Merate, Italy*
[13]*Joint Space-Science Institute, Computer and Space Sciences Building, University of Maryland, College Park, MD 20742, USA*
[14]*INAF, Osservatorio Astronomico di Roma, Via Frascati 33, I-00040 Monteporzio Catone, Italy*
[15]*Space Science Data Center (SSDC), Agenzia Spaziale Italiana (ASI), I-00133 Roma, Italy*
[16]*Department of Physics and Astronomy, Clemson University, Kinard Lab of Physics, Clemson, SC 29634, USA*
[17]*National Science Foundation, Alexandria, VA 22314, USA*
[18]*Center for Space Science and Technology, University of Maryland Baltimore County, 1000 Hilltop Circle, Baltimore, MD 21250, USA*
[19]*DTU Space, National Space Institute, Technical University of Denmark, Elektrovej 327, DK-2800 Kongens Lyngby, Denmark*
[20]*Los Alamos National Laboratory, B244, Los Alamos, NM, 87545, USA*
[21]*Department of Physics and Mathematics, Aoyama Gakuin University, Sagamihara, Kanagawa, 252-5258, Japan*
[22]*Department of Physics and Astronomy, University of Maryland, College Park, MD 20742, USA*

This paper has been typeset from a TEX/LATEX file prepared by the author.